January 1, 2009

Linear Stability of a Volatile Liquid Film Flowing over a Locally Heated Surface

N Tiwari
JM Davis

Linear stability of a volatile liquid film flowing over a locally heated surface

Naveen Tiwari and Jeffrey M. Davis

Citation: Physics of Fluids (1994-present) **21**, 022105 (2009); doi: 10.1063/1.3068757
View online: http://dx.doi.org/10.1063/1.3068757
View Table of Contents: http://scitation.aip.org/content/aip/journal/pof2/21/2?ver=pdfcov
Published by the AIP Publishing

Linear stability of a volatile liquid film flowing over a locally heated surface

Naveen Tiwari and Jeffrey M. Davis[a)]
Department of Chemical Engineering, University of Massachusetts, Amherst, Massachusetts 01003, USA

(Received 23 July 2008; accepted 10 October 2008; published online 17 February 2009)

The dynamics and linear stability of a volatile liquid film flowing over a locally heated surface are investigated. The temperature gradient at the leading edge of the heater induces a gradient in surface tension that leads to the formation of a pronounced capillary ridge. Lubrication theory is used to develop a model for the film evolution that contains three key dimensionless groups: a Marangoni parameter (M), an evaporation number (E), and a measure of the vapor pressure driving force for evaporation (K), which behaves as an inverse Biot number. The two-dimensional, steady solutions for the local film thickness are computed as functions of these parameters. A linear stability analysis of these steady profiles with respect to perturbations in the spanwise direction reveals that the operator of the linearized system can have both a discrete and a continuous spectrum. The continuous spectrum exists for all values of the spanwise wave number and is always stable. The discrete spectrum, which corresponds to eigenfunctions localized around the ridge, appears for values of M larger than a critical value for a finite band of wave numbers separated from zero. Above a second, larger critical value of M, a portion of the discrete spectrum becomes unstable, corresponding to rivulet formation at the forward portion of the capillary ridge. For sufficiently large heat transfer at the free surface, due either to phase change or to convection, a second band of unstable discrete modes appears, which is associated with an oscillatory, thermocapillary instability above the heater. The critical Marangoni parameter above which instability develops, $M_{\mathrm{crit}}(K,E)$, has a nonmonotonic dependence on the steepness of the temperature increase at the heater, in contrast to the monotonic decrease for a nonvolatile film at vanishing Biot number. An energy analysis reveals that the dominant instability mechanism resulting from perturbations to the film thickness is either streamwise capillary flow or gravity for weakly volatile fluids and thermocapillary flow due to spanwise temperature gradients for more volatile fluids. The stability results are rather sensitive to the steepness of the temperature increase and heater width due to the nonlinear coupling of gravity, capillary pressure gradients, thermocapillary flow, and evaporation through the base states. © *2009 American Institute of Physics*. [DOI: 10.1063/1.3068757]

I. INTRODUCTION

Thin liquid films on heated surfaces are important components of many technological applications, including material processing, thermal management of electronic devices, microelectromechanical systems, microfluidic devices, and separation processes. The variation in temperature of a liquid-gas interface results in the formation of a surface-tension gradient, or Marangoni stress.[1] In thin liquid layers, the thermocapillary flow associated with these tangential stresses can lead to significant interfacial deformation, instability, and possible film rupture.[2,3] For liquid films resting on heated, horizontal surfaces, a detailed theoretical analysis has been developed to include the combined effects of thermocapillary instability and evaporation/condensation, vapor recoil, nonequilibrium thermodynamics, and rupture due to long-range van der Waals interactions.[4] This one-sided evaporation model has recently been extended to include a detailed analysis of the vapor diffusion,[5] and other recent studies focus on the influence of wall topography.[6,7]

The stability of a liquid film flowing over a uniformly heated, inclined plane has also been studied extensively. For example, Joo *et al.*[8] developed a model to study the competition of the surface-wave instability due to inertia with thermocapillary and/or evaporative instabilities, which extended the work of Burelback *et al.*[4] to inclined surfaces with gravity-driven flow and hydrostatic pressure. They subsequently expanded this two-dimensional study to examine the nonlinear evolution of three-dimensional heated layers.[9] In particular, they found that the nonlinear interaction of the surface-wave and thermocapillary instabilities lead to longitudinal rolls that, after rupture, evolve into an array of rivulets aligned with the flow. Kalliadasis *et al.*[10] and Trevelyan and Kalliadasis[11] extended these studies with an integral-boundary-layer (IBL) approximation of the Navier–Stokes and energy equations. In contrast to the widely used Benney-type equation,[8,12] which accurately predicts the critical Reynolds number for the long surface-wave instability but breaks down at $O(1)$ Reynolds numbers for isothermal or nonisothermal films,[10] the IBL formulation was found to perform well for moderate Reynolds number but did not accurately predict the critical Reynolds number. Ruyer-Quil *et al.*[13] extended the IBL model using a Galerkin projection with polynomial test functions, yielding a model fully compatible with the Benney expansion up to second order. Scheid *et al.*[14] demonstrated that the linear stability proper-

a)Electronic mail: jmdavis@ecs.umass.edu.

ties of the IBL model are in good agreement with the Orr–Sommerfeld analysis of the Navier–Stokes and energy equations and computed nonlinear solutions for a wide range of parameters, finding that the hydrodynamic and Marangoni instabilities can reinforce each other. Finally, Scheid *et al.*[15] confirmed the validity domain of the Benney equation with Marangoni effects for sufficiently small Reynolds numbers by comparison to a reference IBL model. Most of the results in these studies were restricted to two-dimensional films and not on instabilities that develop from spanwise variations in the free surface.

In addition, flows over inclined planes with nonuniform heating have been studied recently. Scheid *et al.*[16] used long-wave theory to derive an evolution equation for a liquid film falling down a vertical plate with a sinusoidal temperature distribution, which exhibited two instability mechanisms associated with thermocapillarity. These authors found strong agreement between the film shapes predicted by their model and experiments that measured the film thickness profile in the flow direction for localized heating.[17] Demekhin *et al.*[18] studied the Orr–Sommerfeld formulation of the linear stability of a thin liquid film falling down a heated plane with a linear temperature variation. They found two types of transverse instabilities due to hydrodynamic (inertial) and Marangoni instabilities, as for a uniformly heated wall, but with nonuniform heating the thermocapillary forces can either destabilize or stabilize the flow. Miladinova *et al.*[19,20] studied the same problem using the lubrication approximation, performing linear and nonlinear analyses of transverse surface waves. A weakly nonlinear stability analysis in two dimensions was performed for the linear temperature variation by Mukhopadhyay and Mukhopadhyay.[21] Evaporation was included by Miladinova and Lebon,[22] who developed a two-dimensional model for a volatile film flowing over a surface with a periodic temperature profile and focused on the effects of thermocapillarity on the nonlinear evolution of an evaporating, falling film.

While most of these studies were focused on the interaction of the (inertial) surface-wave instability with thermocapillary effects, there has also been much recent theoretical work on pattern formation in liquid films flowing over locally heated surfaces,[23–26] in which interesting dynamics occur even without inertia. These studies were motivated by a series of experiments in which a thin liquid film flows over a plane wall bearing a rectangular heater.[27–29] The temperature gradient at the upstream edge of the heater induces the formation of a two-dimensional bump, or capillary ridge, in the streamwise direction, and the bump height increases with the heat flux from the heater. At a critical value of the heat flux, an instability develops in the transverse direction, and a regular array of longitudinal rivulets forms at the downstream edge of the bump. In subsequent work, Frank and Kabov[25] studied the effect of the Reynolds, Prandtl, Weber, and Biot numbers on the critical Marangoni number (M_{crit}) at instability onset. They used direct numerical simulation to solve the coupled three-dimensional energy and Navier–Stokes equations. Above M_{crit} the flow was found to be unstable for a band of wave numbers separated from zero. This work demonstrated that the rivulet instability occurs even for a Biot number of zero and is thus distinct from the thermocapillary instability of a film flowing over a uniformly heated plate.[9]

There have been several theoretical studies of this instability.[23–26] Skotheim *et al.*[23] used a lubrication analysis of a film flowing over a surface with periodic temperature increases (used to represent an infinite array of heaters). Convection terms were neglected in the momentum and energy equations. Using periodic boundary conditions for the linear stability analysis, they predicted a long-wave instability, i.e., instability for wave numbers in the interval $(0,q_1)$. The flow was always unstable, but a critical Marangoni number was found for the onset of instability by extrapolating the heater periodicity to infinity. The predicted wavelength of the instability was within 20% of experiment, but the critical Marangoni number was about five times too large. Kalliadasis *et al.*[24] studied the stability of a film flowing over a surface with a slowly decaying temperature profile using an IBL approximation of the Navier–Stokes and energy equations for long waves. The convective terms were retained in the energy equation, but the model was solved in the limit of vanishing inertia, which reduced the IBL equations to the usual lubrication approximation without inertia. A linear stability analysis revealed the existence of both a discrete and a continuous spectrum. Like coating flows over surfaces with topographical features[30,31] the continuous spectrum was always stable. Unlike these flows, however, the discrete spectrum was unstable beyond a critical Marangoni number for a band of wave numbers in the interval (q_1,q_2), with $q_1>0$.

Tiwari and Davis[26] subsequently revisited this problem to explain the differences in the qualitative nature of the instability predicted in these two earlier studies.[23,24] They employed a long-wave, lubrication analysis in the limit of vanishing inertia, which is consistent with the work of Skotheim *et al.*[23] The linear stability problem was formulated to allow for disturbances that are bounded (but do not necessarily decay) at the infinities for consistency with the Fourier modes that comprise the continuous spectrum for the flat regions of the film away from the heater, while Skotheim *et al.*[23] employed periodic boundary conditions for both the base state and linear stability analysis. The operator that governs the linearized system was found to have both a discrete and an essential spectrum, in agreement with the results of Kalliadasis *et al.*[24] The essential spectrum consists of eigenfunctions that approach bounded oscillations at the infinities. Although their shape is modified by the capillary ridge near the heater, their corresponding spectrum is described by the dispersion relation of a flat film, and these modes are always stable. An unstable, discrete spectrum exists above a critical Marangoni number for a finite band of wave numbers separated from zero, corresponding to a rivulet instability that is consistent with published results from experiment and direct numerical simulation.[25] Differences in the boundary conditions for the stability analysis were thus found primarily responsible for the qualitative differences between the results of Skotheim *et al.*[23] and Kalliadasis *et al.*[24]

The analysis of Tiwari and Davis[26] was used to predict that the wavelength of the instability, $\lambda_{\max}$, varies with the surface tension σ_0 as $\lambda_{\max}\propto\sigma_0^{1/3}$, which is in good agreement

with the result $\lambda_{max} \propto \sigma_0^{0.365}$ reported by Frank and Kabov.[25] The marginal stability curves predicted by the lubrication model also agree qualitatively with those reported by Frank and Kabov,[25] although differences in the temperature profile at the solid surface and the values of the dimensionless parameters preclude a quantitative comparison. Because the spatial nonuniformity of the base state gives rise to nonnormal (not self-adjoint) linearized operators that govern the evolution of perturbation, Tiwari and Davis[26] also performed a transient, nonmodal analysis to study the short-time dynamics of perturbations. The transient amplification of perturbations was found to be essentially negligible for unstable wave numbers because the (unstable) discrete eigenfunction is nearly orthogonal to the (stable) continuous modes. Weak transient amplification was found for stable wave numbers, indicating that nonmodal effects are insignificant for noninertial flows over locally heated surfaces in the limit of vanishing Biot number.

In this present paper, the analysis of spanwise rivulet formation in thin liquid films flowing over a locally heated wall is extended to account for significant heat transfer from the free surface due to either convection or evaporation. The lubrication approximation is used to reduce the Navier–Stokes and energy equations and free-surface boundary conditions to a nonlinear partial differential equation for the evolution of the local height of the free surface in Sec. II. This model corresponds to the limit of vanishing inertia for the Benney and IBL approximations[10] and is consistent with the approaches of Skotheim *et al.*,[23] Kalliadasis *et al.*,[24] and Tiwari and Davis.[26] Steady, two-dimensional film profiles are computed in Sec. III A. For sufficiently strong evaporation, the unperturbed base state ruptures at the heater. For weaker evaporation, the linear stability of the two-dimensional ridge to spanwise perturbations is examined in Sec. III B. The critical values of the Marangoni parameter above which instability develops are computed for a range of parameter space, and the shapes of the eigenfunctions are presented for qualitatively different rivulet and thermocapillary instabilities. In Sec. III C, the influence of the steepness of the temperature increase at the heater on the critical Marangoni parameter is investigated and shown to be much more significant than for the limit of vanishing Biot number investigated previously.[26] An energy analysis is presented in Sec. III D to gain insight into the destabilizing mechanisms for different values of the governing dimensionless groups. The results of this study are compared with those from previous work in Sec. IV. Conclusions are presented in Sec. V.

II. PROBLEM FORMULATION

Consider a thin liquid film with density ρ, kinematic viscosity ν, and thermal diffusivity α_{th} flowing under the influence of gravity over a planar substrate inclined from the horizontal by angle θ. The film flows along the plane in the $\hat{x}$ direction, $\hat{z}$ is directed outwardly normal from the substrate, and $\hat{y}$ is the transverse coordinate in the plane of the substrate. A rectangular heater is embedded in the substrate, as shown schematically in Fig. 1, and generates the temperature profile $\hat{T}_0(\hat{x})$ at the solid surface. Far upstream of the heater, the film has constant thickness $\hat{h}=\hat{h}_\infty$, corresponding to the liquid being supplied at a constant flow rate.

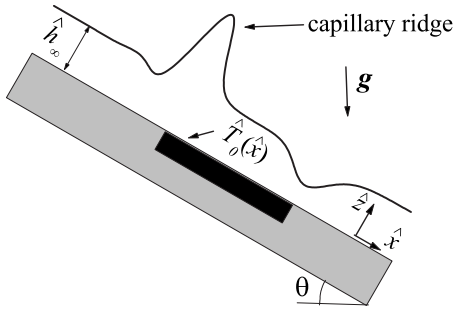

FIG. 1. Schematic of a thin liquid film flowing over a heater. The Marangoni stress at the edge of the heater opposes the gravitational flow, which leads to the formation of a capillary ridge.

A. Dimensional equations

The velocity ($\hat{\boldsymbol{u}}$), pressure ($\hat{p}$), and temperature ($\hat{T}$) fields are governed by the Navier–Stokes equation,

$$\hat{\boldsymbol{u}}_t + \hat{\boldsymbol{u}} \cdot \nabla \hat{\boldsymbol{u}} = \frac{-1}{\rho} \nabla \hat{p} + \nu \nabla^2 \hat{\boldsymbol{u}} + \boldsymbol{g}, \tag{1}$$

the continuity equation for an incompressible fluid,

$$\nabla \cdot \hat{\boldsymbol{u}} = 0, \tag{2}$$

and the energy equation,

$$\hat{T}_t + \hat{\boldsymbol{u}} \cdot \nabla \hat{T} = \alpha_{th} \nabla^2 \hat{T}. \tag{3}$$

Dimensional variables are denoted by $\hat{\cdot}$. The localized heating prescribes the temperature profile at the solid surface,

$$\hat{T}(\hat{x}, \hat{y}, \hat{z} = 0) = \hat{T}_0(\hat{x}). \tag{4}$$

At the plate surface, the no-slip and no-penetration boundary conditions are enforced,

$$\hat{\boldsymbol{u}}|_{\hat{z}=0} = \boldsymbol{0}. \tag{5}$$

The normal and tangential stress balances at the free surface, $\hat{z}=\hat{h}(\hat{x},\hat{y},\hat{t})$, are

$$\boldsymbol{n} \cdot \hat{\boldsymbol{\Gamma}} \cdot \boldsymbol{n} = \sigma(\nabla_s \cdot \boldsymbol{n}), \tag{6}$$

$$\boldsymbol{t} \cdot \hat{\boldsymbol{\Gamma}} \cdot \boldsymbol{n} = -\boldsymbol{t} \cdot \nabla_s \sigma, \tag{7}$$

where $\hat{\boldsymbol{\Gamma}}$ is the stress tensor for a Newtonian fluid of viscosity μ and σ is the liquid-gas surface tension. The unit vectors normal and tangent to the liquid-gas interface are denoted $\boldsymbol{n}$ and $\boldsymbol{t}$, respectively, and vapor recoil[4] is neglected in this analysis.

B. Interfacial heat transfer

The treatment of heat transfer from the liquid to the surrounding air requires some discussion. In the work of Burelbach *et al.*[4] and many subsequent studies, the model of the liquid film dynamics was formulated using the assumption that evaporation is governed by the departure from thermo-

dynamic equilibrium at the liquid-gas interface, which leads to an expression for the evaporation rate based on kinetic theory,

$$\hat{J} = \left(\frac{\alpha \rho^v \Delta H_{\text{vap}}}{\hat{T}_\infty^{3/2}}\right)\left(\frac{M_w}{2\pi R_g}\right)^{1/2}(\hat{T}^i - \hat{T}_\infty). \tag{8}$$

In Eq. (8) ΔH_{vap} is the latent heat of vaporization, M_w is the molecular weight, R_g is the universal gas constant, ρ^v is the vapor density, and α is a dimensionless accommodation coefficient in the kinetic theory that accounts for deviations from ideal behavior due to interface/molecular orientation and steric effects.[1] Typically, $\alpha \approx 1$ is used.[4] In this one-sided model, mass transfer (diffusion) of the vapor is assumed to be very fast, corresponding to the limit of large Peclet number in the gas phase.[5] Consequently, the vapor density is spatially uniform, and the evaporation rate is determined only from thermodynamic considerations at the liquid-vapor interface.

In many situations, the rate of mass transfer of the vapor from the interface limits the evaporation rate. Sultan *et al.*[5] developed a theoretical model to study the stability of an evaporating, thin liquid film on a solid substrate. Their analysis accounts for the influence of the rate of vapor diffusion away from the interface on the evaporation rate of the liquid film. Motivated by studies of evaporating droplets,[32–35] they studied the diffusion-limited regime (in addition to the one-sided model of Burelbach *et al.*[4]). This approach entailed solving the Laplace equation for the vapor density field, which was coupled to a lubrication equation for the evolution of the evaporating liquid film.

It has been indicated in many studies of evaporation that the evaporation rate derived from kinetic theory may be significantly larger than the measured value. The empirical evaporation coefficient ε_E was introduced as a multiplicative factor on the right-hand side of Eq. (8) to correlate experimental measurements,[36] but the reported values vary widely for nominally similar experimental conditions.[37] For example, the reported evaporation coefficient of water at 1 atm and 20–50 °C ranges from 0.0002 to 0.3.[37] In addition, small evaporation coefficients are common for polar liquids, and the presence of trace impurities at a liquid-gas interface significantly lowers the evaporation coefficient, which is especially significant for water because of the high dipole moment.[37] Because of this wide variation of ε_E, a range of values is used below to estimate the dimensionless parameters in the present study.

Furthermore, to incorporate the important physics of situations in which mass transfer in the vapor phase limits the evaporation rate while avoiding the mathematical complexity of coupling the nonlinear lubrication equation to a detailed treatment of the vapor-phase transport for the case of a spatially varying free-surface shape, a simplified derivation is given below in which a mass-transfer coefficient is utilized to account for transport of the vapor away from the interface. The resulting expression for the evaporation rate (in dimensionless form) is shown to be identical to that based on the one-sided model of Burelbach *et al.*,[4] although the admissible range of the governing dimensionless parameter K, which is defined in Eq. (30) below, is larger.

The consideration of these seemingly large values of K is further supported by several authors (e.g., Anderson and Davis[38]) who associated the value of K with the inverse of the Biot number and argued that larger values of K (than calculated from the kinetic theory) are relevant for these evaporating films. Consideration of the larger range of K in the results below further allows a smooth transition from the regime of a highly volatile liquid, which corresponds to a large heat transfer rate from the free surface to the case of a nonvolatile liquid, which corresponds to a very small rate of heat transfer (small Biot number for these thin films). This reasoning would also explain the strong agreement between theoretical studies based on a nonvolatile fluid[16,23,25] (the $K \to \infty$ limit) and experiments[17,25,28] with water and ethanol that would correspond to $K < 1$ as calculated from the kinetic theory result (one-sided model of Burelbach *et al.*[4]) with an evaporation coefficient of unity.

1. One-sided evaporation limit

The mass balance at the interface $[\hat{z} = \hat{h}(\hat{x}, \hat{y}, \hat{t})]$ is given by

$$\hat{J} = \rho(\hat{\boldsymbol{u}} - \hat{\boldsymbol{u}}^i) \cdot \boldsymbol{n}, \tag{9}$$

where $\hat{\boldsymbol{u}}^i$ is the velocity of the interface and $\hat{J}$ is the mass flux across the interface. It is assumed in these boundary conditions that the density, viscosity, and thermal conductivity of the liquid are much greater than those of the vapor in this one-sided model,[4] which allows the formulation of effective boundary conditions for the liquid phase without solving for the flow and heat transfer in the vapor. With these simplifications, as noted by Oron *et al.*,[1] the energy balance at $\hat{z} = \hat{h}$ reduces to

$$\hat{J}\Delta H_{\text{vap}} = -k\boldsymbol{n} \cdot \nabla \hat{T}, \tag{10}$$

where ΔH_{vap} is the latent heat of vaporization and k is the thermal conductivity for the liquid. It is therefore assumed that all the heat conducted across the liquid film to the interface is converted to latent heat of evaporation. Because $\hat{J}$ is related to $\hat{T}^i - \hat{T}_\infty$ with a linearized constitutive equation in the following sections, heat transfer from the interface to the surrounding gas via convection, which can be modeled using a heat transfer coefficient, could be easily incorporated into Eq. (10) by adding a term $k_H(\hat{T}^i - \hat{T}_\infty)$ to the left-hand side, where k_H is the heat transfer coefficient, and adjusting the definition of the parameter K slightly in what follows.

Following Burelbach *et al.*[4] and Maa[39] the interfacial temperature $\hat{T}^i$ is related to the mass flux using a linearized constitutive equation,

$$\hat{J} = \left(\frac{\varepsilon_E \rho^v \Delta H_{\text{vap}}}{\hat{T}_\infty^{3/2}}\right)\left(\frac{M_w}{2\pi R_g}\right)^{1/2}(\hat{T}^i - \hat{T}_\infty). \tag{11}$$

Equation (11) can be derived using kinetic theory assuming ideal gas behavior,[40] in which the film heat transfer coefficient at the liquid-vapor interface is related to properties of

the vapor at saturation conditions.[39] The dimensionless, empirical evaporation coefficient[37] ε_E was defined[39] as the ratio of the observed to calculated evaporation rate and has been used to correlate a large number of measurements.[36] This coefficient has been shown to be a small parameter $\varepsilon_E < 1$, with reported values for water ranging from 0.0002 to 0.3 in many experimental studies.[37]

2. Evaporation limited by vapor transport

For mass-transfer-limited evaporation for which the gas phase is saturated in vapor in the vicinity of the interface,[5] the evaporation rate is equal to the rate at which vapor is transported away from the interface,

$$\hat{J} = k_m(\rho^v|_{\text{int}} - \rho^v_\infty), \tag{12}$$

where k_m is the mass-transfer coefficient, $\rho^v|_{\text{int}}$ is the vapor density at the interface, and ρ^v_∞ is the vapor density in the bulk gas away from the interface as $\hat{z} \to \infty$. The use of k_m to characterize the vapor transport away from the interface is analogous to using a heat transfer coefficient to model convection in the gas phase. For small differences between $\hat{T}^i$ and $\hat{T}_\infty$, a Taylor series expansion of $\rho^v(\hat{T})$ about $\hat{T}_\infty$ yields

$$\rho^v|_{\text{int}} = \rho^v_\infty + \left.\frac{d\rho^v}{d\hat{T}}\right|_{\hat{T}_\infty} (\hat{T}^i - \hat{T}_\infty). \tag{13}$$

Equation (12) then reduces to

$$\hat{J} = k_m \frac{d\rho^v|_{\text{int}}}{d\hat{T}} (\hat{T}^i - \hat{T}_\infty). \tag{14}$$

Using the Clausius–Clapeyron equation,[41]

$$\frac{1}{p^v}\frac{dp^v}{d\hat{T}} = \frac{\Delta H_{\text{vap}} M_w}{R_g \hat{T}^2_\infty}, \tag{15}$$

and the ideal gas law, $\rho^v(\hat{T}_\infty) = p^v M_w/(R_g T_\infty)$,

$$\frac{d\rho^v}{d\hat{T}} = \frac{\rho^v M_w \Delta H_{\text{vap}}}{R_g \hat{T}^2_\infty}. \tag{16}$$

Substituting Eq. (16) into Eq. (14) yields a linearized equation for the evaporative mass flux,

$$\hat{J} = \frac{k_m \rho^v|_{\text{int}} M_w \Delta H_{\text{vap}}}{R_g \hat{T}^2_\infty} (\hat{T}^i - \hat{T}_\infty), \tag{17}$$

which is combined with Eq. (10) to provide a boundary condition for the temperature field at $\hat{z} = \hat{h}(\hat{x}, \hat{y}, \hat{t})$.

3. Convective heat transfer

For a nonvolatile liquid, heat transfer from the free surface to the surrounding gas is characterized by a heat transfer coefficient k_H,

$$-k\boldsymbol{n} \cdot \nabla \hat{T} = k_H(\hat{T} - \hat{T}_\infty) \quad \text{at} \quad \hat{z} = \hat{h}(\hat{x}, \hat{y}). \tag{18}$$

C. Dimensionless equations

The governing equations are made dimensionless by introducing the new variables

$$(z,h) = (\hat{z},\hat{h})/\hat{h}_\infty, \quad (x,y) = (\hat{x},\hat{y})/l_c,$$

$$T = (\hat{T} - \hat{T}_\infty)/\Delta\hat{T}, \quad p = \hat{p}/[\sigma_0 \text{Ca}/\hat{h}_\infty],$$

$$l_c = \hat{h}_\infty (3\text{Ca})^{-1/3}, \quad \text{Ca} = \mu U/\sigma_0 \tag{19}$$

$$U = (\rho g \hat{h}^2_\infty \sin\theta)/(3\mu), \quad \Delta\hat{T} \equiv \hat{T}_H - \hat{T}_\infty,$$

$$M = 3^{1/3}\sigma_T \Delta T/(2\sigma_0 \text{Ca}^{2/3}), \quad J = \hat{J}(\Delta H_{\text{vap}} \hat{h}_\infty/k\Delta\hat{T}),$$

where l_c is the dynamic capillary length, Ca is the capillary number, U is the characteristic velocity of the film, $\hat{T}_H$ is the maximum temperature at the heater, and σ_0 is the surface tension of the liquid at the ambient temperature, $\hat{T} = \hat{T}_\infty$. A linear variation of surface tension with temperature is assumed, i.e., $\sigma(\hat{T}) = \sigma_0 - \sigma_T(\hat{T} - \hat{T}_\infty)$ where $\sigma_T > 0$ and $\sigma_T \equiv \partial\sigma/\partial\hat{T}$. The Marangoni parameter M quantifies the magnitude of the surface-tension gradient from the nonuniform temperature profile at the heater. The resulting dimensionless equations are reduced to a more tractable form by invoking the lubrication approximation,[1] which in this case requires $\text{Ca}^{2/3} \ll 1$, $\text{ReCa}^{1/3} \ll 1$, and $\text{PeCa}^{1/3} \ll 1$, where $\text{Re} = U\hat{h}_\infty/\nu$ is the Reynolds number and $\text{Pe} = U\hat{h}_\infty/\alpha_{\text{th}}$ is the Peclet number. Only the leading-order equations are given below.

1. Momentum equations

With these simplifications, the scalar components of Eq. (1) reduce to

$$u_{zz} = p_x - 3, \tag{20}$$

$$v_{zz} = p_y, \tag{21}$$

$$p_z = -3G, \tag{22}$$

where (u,v,w) are the dimensionless components of the velocity in the (x,y,z) directions, respectively. The parameter that characterizes the importance of hydrostatic pressure is $G = (3\text{Ca})^{1/3}\cot\theta$.

In dimensionless form, the no-slip condition at the solid surface, Eq. (5), is

$$\boldsymbol{u}|_{z=0} = 0. \tag{23}$$

At $z = h(x,y,t)$, the normal and tangential stress balances in Eqs. (6) and (7) reduce to

$$P(z=h) = -\nabla^2 h \tag{24}$$

and

$$\boldsymbol{u}_z(z=h) = -2M\nabla T^i, \tag{25}$$

where $T^i=(\hat{T}^i-\hat{T}_\infty)/\Delta\hat{T}$ is the dimensionless temperature field at the interface that is found from the energy equation. Solving Eqs. (20)–(22) using the boundary conditions given by Eqs. (23)–(25), the velocity vector field in the x-y plane is

$$\boldsymbol{u}_\parallel = 3(\boldsymbol{e}_x + \nabla\nabla^2 h - G\nabla h)\frac{[h^2-(z-h)^2]}{2} - 2M\nabla T^i z. \tag{26}$$

2. Energy equation

At leading order, Eq. (3) simplifies to

$$T_{zz} = 0, \tag{27}$$

with the streamwise convection of energy neglected at $O(\mathrm{PeCa}^{1/3})$. At the solid surface, a prescribed temperature profile, $T_0(x)$, is assumed to be generated by the localized heating,

$$T(z=0) = T_0(x). \tag{28}$$

The boundary condition at the free surface, $z=h(x,y)$, accounts for heat loss to the surrounding gas. For a volatile liquid, heat transfer is assumed to be dominated by evaporation. For a nonvolatile liquid, the heat loss is modeled using a heat transfer coefficient, as detailed below. Finally, the dimensionless mass flux at the interface, J, is obtained from Eq. (10),

$$J = -T_z^i. \tag{29}$$

3. One-sided evaporation model

The nonequilibrium condition at the interface given by Eq. (11) is reduced to

$$KJ = T^i, \tag{30}$$

where $K=[k\hat{T}_\infty^{3/2}(2\pi R_g/M_w)^{1/2}/\varepsilon_E\hat{h}_\infty\rho^v\Delta H_{\mathrm{vap}}^2]$. The parameter K represents (in the linear approximation) the vapor pressure driving force for mass transfer from the interface.[1] Because the mass flux (evaporation) is linked to heat transfer through ΔH_{vap}, K also behaves as an inverse Biot number that quantifies the resistance to heat transfer from the free surface to the surrounding gas relative to the thermal resistance from conduction across the liquid film.[39]

Because reported values of ε_E vary widely and to model liquid films of varying thickness and physical properties, a wide range of values is taken for the parameter K. The range $0.1\le K\le 10$ is emphasized because it corresponds to the richest film dynamics and also corresponds to realistic situations and attainable values of the Biot number at the higher end of this range ($1/K=\mathrm{Bi}$ with no evaporation). (The larger values of K in this range correspond to the Biot numbers studied by Skotheim *et al.*,[23] so relevant comparisons to their analysis can be made for consistent parameter values.) As an example of representative values, at $T_\infty=25\ ^\circ\mathrm{C}$ and 1 atm, for a water film of $\hat{h}_\infty=10$–$50\ \mu\mathrm{m}$ and assuming[37] $\varepsilon_E=0.02$, $K\approx 2$–10. For the specialty liquids FC-72 and FC-77 that are used as coolants, assuming $\varepsilon=0.1$, for $\hat{h}_\infty=10\ \mu\mathrm{m}$, $K=0.12$ and 0.52, respectively. As shown in Sec. III B below, flowing films with such small value of K become stable to rivulet formation and thermocapillary instabilities, making such liquids well suited for heat removal. For a low-volatility liquid (or a contaminated interface), the vapor density is very low and the evaporation coefficient ε_E can be very small due to a large molecular attraction at the liquid-vapor interface;[37] hence K can be relatively large.

The dimensionless temperature profile at the interface is obtained by integrating Eq. (27) and using Eqs. (28) and (29) as boundary conditions,

$$T^i = \frac{KT_0}{(K+h)}. \tag{31}$$

The dimensionless mass flux J is then

$$J = \frac{T_0}{(K+h)}. \tag{32}$$

From Eq. (32) it can be seen that $J\to 0$ as $K\to\infty$, corresponding to no evaporation, which is the only mechanism for heat transfer from the free surface to the surrounding gas in this model. Consequently, $T^i\to T_0$ as $K\to\infty$ from Eq. (31), which corresponds to the limit of vanishing Biot number investigated previously.[26] Physically, the free surface behaves as a no-flux boundary [$T_z^i=0$ from Eq. (29) since $J\to 0$]. There is no vertical temperature gradient in the liquid film, and the temperature is everywhere identical to that of the heated substrate. The limit $K\to 0$ implies that $T^i=0$, which corresponds to the quasiequilibrium state with the interfacial temperature always the same as the surrounding gas due to rapid heat transfer by evaporation. In this limit of large effective heat transfer coefficient, the free surface is a perfect conductor, and the temperature along the surface is the constant ambient temperature. As noted by Joo *et al.*[8] for a uniformly heated surface, the thermocapillary instability disappears in these two distinct limits of either $K\to 0$ or $K^{-1}\to\infty$. The film may still be susceptible to a rivulet instability[26] for $K\to\infty$ because the nonuniform heating induces a thermocapillary ridge at the heater, but the film is also stable to the rivulet instability for $K\to 0$ because with an isothermal interface ($T^i=0$), there is no distortion of the free surface.

4. Evaporation limited by vapor transport

Introducing the dimensionless variables given by Eq. (19), Eq. (17) reduces to

$$KJ = T^i, \tag{33}$$

where $K=kR_g\hat{T}_\infty^2/k_m\rho^v\hat{h}_\infty M_w\Delta H_{\mathrm{vap}}^2$. Equation (33) is thus identical to Eq. (30) with a different definition of the parameter K, so the subsequent development in Sec. II C 3 applies also to the transport-limited case with the appropriate redefinition of K. For a water film of thickness $\hat{h}_\infty=50\ \mu\mathrm{m}$ with $\hat{T}_\infty=25\ ^\circ\mathrm{C}$ and taking $k_m=0.04$ m/s to be a representative value in a gas phase contacting a flowing liquid film,[42] $K\approx 200$. Note that k_m could be larger if convection in the gas phase is increased, and K would be much smaller for a more volatile liquid. If $k_m\to\infty$ then thermodynamic effects at the

TABLE I. Definition and physical interpretation of dimensionless groups.

Parameter	Definition	Physical interpretation
Re	$\rho U\hat{h}_\infty/\mu$	Ratio of inertia to viscous forces
Ca	$\mu U/\sigma_0$	Ratio of viscous force to surface-tension force
Pe	$U\hat{h}_\infty/\alpha_{\text{th}}$	Ratio of convective heat transfer in flowing film to conduction across film
M	$3^{1/3}\sigma_T\Delta T/(2\sigma_0\ \text{Ca}^{2/3})$	Dimensionless surface-tension gradient
K	$k\hat{T}_\infty^{3/2}(2\pi R_g/M_w)^{1/2}/(\alpha\hat{h}_\infty\rho^v\Delta H_{\text{vap}}^2)$	Dimensionless vapor pressure driving force for net mass transfer from free surface; also, ratio of heat transfer resistance between free surface and surrounding gas to thermal resistance from conduction across liquid film
E	$k\Delta\hat{T}/(\rho U\hat{h}_\infty\Delta H_{\text{vap}})$	Ratio of convective time scale to evaporative time scale

interface must be taken into account as in the one-sided model.

5. Convective heat transfer

Without evaporation, the energy balance at the liquid-vapor interface, Eq. (18), is written in dimensionless form as

$$-\frac{\partial T}{\partial z}=\text{Bi}\,T \quad \text{at} \quad z=h(x,y), \tag{34}$$

where $\text{Bi}=\hat{h}_\infty k_H/k$ is the Biot number. Integrating Eq. (27) and using the boundary conditions in Eqs. (28) and (34), the interfacial temperature is

$$T^i=\frac{T_0}{1+\text{Bi}\,h}. \tag{35}$$

With the substitution $K=\text{Bi}^{-1}$, Eq. (35) is identical to Eq. (31).

6. Evolution equation

Using the scaled kinematic condition derived from Eq. (9),

$$\frac{\partial h}{\partial t}+\ w|_{z=h}+\nabla\cdot\int_0^h \boldsymbol{u}_\parallel dz=0, \tag{36}$$

where w is the dimensionless liquid velocity in the z direction, and Eq. (26), an equation governing the evolution of the interface shape, is obtained,

$$\frac{\partial h}{\partial t}+EJ+\nabla\cdot[(\boldsymbol{e}_x+\nabla\nabla^2 h-G\,\nabla\,h)h^3-M\,\nabla\,T^i h^2]=0. \tag{37}$$

Here, $E=(k\Delta\hat{T})/(\rho U\hat{h}_\infty\Delta H_{\text{vap}})$ is a dimensionless evaporation number that is a ratio of the convective time scale, $t_c=\hat{h}_\infty/U$, to the evaporative time scale, $t_e=(\rho h_\infty^2\Delta H_{\text{vap}})/(k\Delta\hat{T})$, which is a measure of the time required for the complete evaporation of a stationary liquid film on a heated, horizontal wall. In the remainder of this work, attention is restricted to a vertical substrate, $\theta=\pi/2$, so $G=0$. For a water film of thickness $\hat{h}_\infty=50$ μm with $\Delta\hat{T}=20$ °C, $E=0.0016$. Because $E\propto\hat{h}_\infty^{-3}$, an order of magnitude change in the film thickness results in a three order of magnitude change in E, so a wide range of parameter values is considered below. In the limit $E\to 0$ with the substitution $K=\text{Bi}^{-1}$, the results for a nonvolatile film (with heat loss by convection) are recovered. The key dimensionless parameters and their physical interpretation are summarized in Table I.

The boundary conditions for Eq. (37) are that the film is uniform away from the heater,

$$\begin{aligned} &h\to 1, \quad h_x\to 0 \quad \text{as} \quad x\to-\infty,\\ &h\to c_1, \quad h_x\to 0 \quad \text{as} \quad x\to\infty, \end{aligned} \tag{38}$$

where $0<c_1\leq 1$ to allow for mass loss to evaporation while the film flows over the heater.

Without evaporation ($E=0$), the evolution equation for the nonisothermal film given by Eq. (37) is the same as the one derived by Skotheim *et al.*[23] with $K\equiv\text{Bi}^{-1}$ and a different choice of scalings. The use of the dynamic capillary length l_c as the characteristic length scale in the x and y directions in this work places a parameter in the boundary conditions (temperature profile) rather than in the governing partial differential equation,[26] as in Ref. 23. Such a choice is analogous to studies of a liquid film flowing over a substrate bearing topographical features.[43] Aside from evaporation, the key differences between the present work and that of Skotheim *et al.*[23] are the more general bounded conditions in the stability analysis below (for consistency with the continuous spectrum of the flat-film regions) instead of periodic boundary conditions and studying a single, localized region of heating rather than a periodic array of temperature increases. Similar evolution equations have been derived in many previous studies. For example, Joo *et al.*[8] derived a more general (two-dimensional) evolution equation for flow over a homogeneously heated surface that also included the effects of inertia, vapor recoil, and higher order terms due to evaporation, which formed the basis for many subsequent studies. Scheid *et al.*[16] derived a similar evolution equation that included inertial effects but neglected evaporation. Without evaporation, Eq. (37) is consistent with the limit of the IBL approximation solved by Kalliadasis *et al.*[24] for flow over a locally heated surface, although those authors also retained the convective term in the energy equation. Also, Miladinova and Lebon[22] used a two-dimensional model

similar to that of Joo *et al.*[8] that included inertia and higher order evaporation terms to study flow over a surface with a periodic temperature profile.

III. RESULTS

A. Base profiles

The steady, two-dimensional base profile is found by seeking solutions of the form $h(x,y,t)=h_0(x)$. Making this substitution into Eq. (37) yields

$$\frac{ET_0}{(K+h_0)}+\frac{\partial}{\partial x}[(1+h_{0xxx})h_0^3-MT_{0x}^i h_0^2]=0. \tag{39}$$

The base states were computed for a finite-domain, $x\in[-L,L]$ with $h_0(x=-L)=1$, $h_{0x}(x=-L)=0$, $h_{0x}(x=L)=0$, and $h_{0xxx}(x=L)=0$. Neumann boundary conditions were applied at $x=L$ to allow for the mass loss due to evaporation at the heater. The domain length was chosen such that neither the base state nor the linear stability results changed upon increasing the domain size further, which required $L\geq 40$ ($L\approx 80$ in some cases) because some of the eigenfunctions for discrete modes decay slowly as $x\to\infty$. Finite element computations were performed using FEMLAB 3.1 to determine the base profiles for different values of M, K, and E, with a prescribed temperature field $T_0(x)$ at the solid surface. It was found expedient to retain the time dependence of h in Eq. (39) for computational purposes. A unit height profile was chosen as the initial condition, and Eq. (39) was evolved in time until a steady profile was obtained. The accuracy of the method was assessed by examining the invariance of $\int_{-\infty}^{\infty}[MT_x^i/h_0+(1-h_0^3)/h_0^3]dx=0$ for $E=0$. This property is guaranteed from Eq. (39) and its boundary conditions, and the value of this integral was always less than 10^{-9}. Other tests of accuracy included convergence after mesh refinement and variation of the integration interval. Typically, about 2000 points were used for the computations, with local refinement of the mesh around the regions with steep gradients in the temperature or free-surface shape.

The heater embedded in the substrate is modeled as

$$T_0(x)=0.5\{\tanh[\omega(x+\chi)]-\tanh[0.5(x-8)]\}, \tag{40}$$

where ω is a parameter that governs the steepness of the temperature increase at the upstream edge of the heater and χ governs the streamwise extent of the heater. Tiwari and Davis[26] found that χ has essentially no effect on the shape of the capillary ridge or stability results for a nonvolatile film with $\mathrm{Bi}\to 0$, while the height of the capillary ridge increases with ω. The film becomes unstable to rivulet formation above a critical value of the Marangoni parameter M_{crit}^r, which decreases as ω increases for a nonvolatile film.[26] Tiwari and Davis[26] also found that the height of the ridge and M_{crit}^r both saturate for $\omega\geq 5$. For a volatile film, the case $\omega=1$ and $\chi=8$ is first considered to explore the unperturbed film profile and structure of the eigenspectrum, and the effect of changing ω and χ is presented in Sec. III C below.

Shown in Fig. 2(a) are base profiles for different values of E with $M=15$ and $K=3$. The temperature profile is superimposed as the dotted curve and rescaled for clarity. These profiles are obtained by solving Eq. (39) with Eq. (40) and

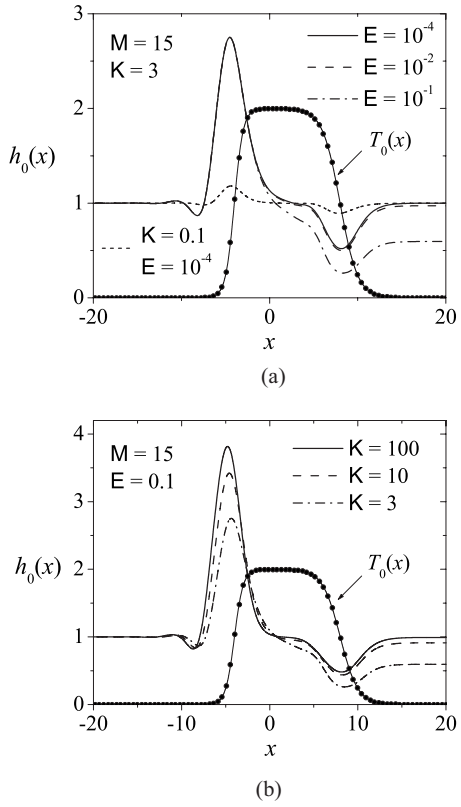

FIG. 2. Base profiles for $M=15$. The temperature profile $T_0(x)$ is scaled by a factor of 2 in this figure for clarity. (a) $K=3$ for different values of E. (b) $E=0.1$ for different values of K.

$\omega=1$. Because $dT_0/dx>0$ at the upstream edge of the heater, $d\sigma/dx<0$. The resulting Marangoni stress decreases the streamwise velocity near the free surface, the film thickens in this region to maintain a constant flow rate, and this local thickening is smoothed by surface tension into a capillary ridge. This ridge increases in amplitude as M increases and is susceptible to the formation of periodic rivulets aligned with the flow beyond a critical value of the Marangoni parameter M_{crit}. At the downstream edge of the heater, $d\sigma/dx>0$, and there is a depression in the free surface. The magnitude of the depression has a weaker dependence on M than that of the ridge and was found to have a minimal influence on the stability results. As E increases, the evaporative flux at the heater increases, and the film thins as it flows downstream, with $h_0\to\mathrm{const}<1$ as $x\to\infty$. For $K=0.1$ the distortions to the film shape from $h_0=1$ are small because $T^i\approx 0$ due to the large heat loss from the film.

Base profiles are plotted in Fig. 2(b) for $M=15$ and $E=0.1$ for different K, which corresponds to liquids with different volatilities. For large K, the evaporative mass flux is small, as seen from Eq. (32). For example, with $K=100$ the evaporative mass flux is almost negligible, as $h_0\approx 1$ at $x=20$ in Fig. 2(b). Furthermore, because heat transfer from the free surface is assumed to be dominated by evaporation, $T^i\approx T_0$ for large K from Eq. (31). The capillary ridge induced by the Marangoni stress at the heater is therefore largest for large K, which corresponds to the limit of vanishing Biot number for a nonvolatile film investigated previously.[26] As K is decreased, the evaporative mass flux increases, and the

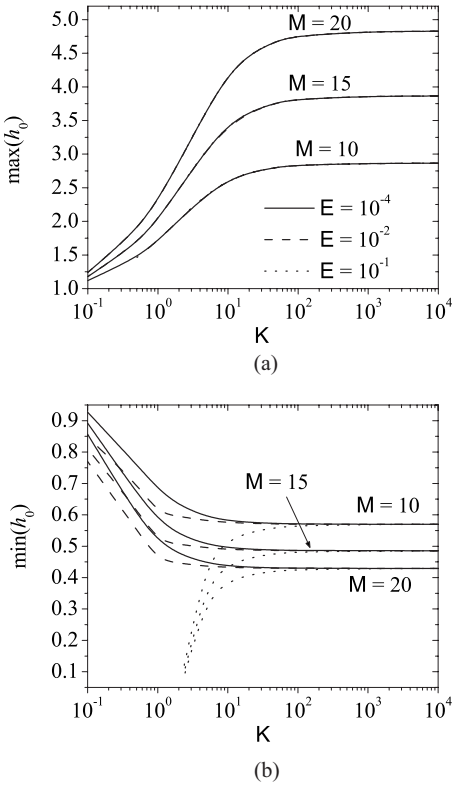

FIG. 3. (a) Effect of evaporation on maximum height of the base profile. The curves for different E are indistinguishable. (b) Effect of evaporation on minimum height of the base profile. The film ruptures at the heater for $E=0.1$ and $K\leq 2$.

streamwise temperature gradient at the free surface decreases in magnitude. Consequently, films with smaller K lose more mass to evaporation and have smaller capillary ridges, as seen in Fig. 2(b) for $K=3$, which corresponds to a highly volatile liquid.

The influences of E, K, and M on the thickness of the capillary ridge and depression are plotted in Fig. 3. The height of the ridge increases with M due to an increase in the Marangoni stress. Likewise, the height of the depression decreases with M. As shown in Fig. 3(a), E has essentially no influence on the height of the capillary ridge. Evaporation occurs only for $T_0>0$ and is thus restricted to the region of the film above the heater, while the peak of the capillary ridge is located at the upstream edge of the heater where $J\approx 0$. The maximum height of the ridge increases monotonically with K and asymptotes for $K\to\infty$, corresponding to no heat transfer from the free surface and $T^i=T_0$, as explained above.

As shown in Fig. 3(b), the minimum thickness of the film at the downstream edge of the heater has a strong dependence on E because of the competition between mass loss to evaporation and the Marangoni stress. For $E=10^{-4}-10^{-2}$, $\min(h_0)$ decreases as K increases and asymptotes to a constant value as $K\to\infty$. This decrease occurs because the Marangoni stress at the downstream edge of the heater, which is aligned with the gravitational flow, increases with K, and the film thins to maintain a constant flow rate. For $E=0.1$, however, $\min(h_0)$ decreases as K decreases. While the Marangoni stress decreases as K decreases because T_x^i decreases, as seen from Eq. (31), the evaporative mass flux increases, as seen from Eq. (32). Evaporation occurs above the entire heater since $T_0>0$, and the film ruptures [i.e., $\min(h_0)=0$] at the downstream edge of the heater for sufficiently small K ($K\approx 2$), as is evident in Fig. 3(b). The minimum in the film thickness decreases as M increases because of the larger Marangoni stress that reinforces the gravity-driven flow. It will be shown in the next section via a linear stability analysis that the base states for small K can lead to an oscillatory, thermocapillary instability because of the large heat transfer by evaporation.

B. Linear stability

In order to investigate the stability of these two-dimensional solutions to perturbations that vary in the transverse direction, a small perturbation to the film thickness is imposed, $h(x,y,t)=h_0(x,t)+\epsilon h_1(x,t)\exp(iqy)$, with $\epsilon\ll 1$. Upon substitution into Eq. (37) and collecting $O(\epsilon)$ terms, the linearized equation governing the evolution of perturbations is obtained,

$$\frac{\partial h_1}{\partial t}=\sum_{i=0}^{i=4}\mathbb{L}_i h_1, \tag{41}$$

where

$$\mathbb{L}_0=-\{3[h_0^2(1+h_{0xxx})]_x-ET_0/(K+h_0)^2-2M(T_{0x}^i h_0)_x - M(T_{1x}^i h_0^2)_x+q^2MT_1^i h_0^2+q^4h_0^3\},$$

$$\mathbb{L}_1=-[3h_0^2(1+h_{0xxx})-3q^2h_0^2h_{0x}-2MT_{0x}^i h_0-MT_{1x}^i h_0^2 - M(T_1^i h_0^2)_x],$$

$$\mathbb{L}_2=-[-2q^2h_0^3-Mh_0^2T_1^i], \tag{42}$$

$$\mathbb{L}_3=-3h_0^2h_{0x},$$

$$\mathbb{L}_4=-h_0^3.$$

Due to the perturbation in h, the interfacial temperature profile, given by Eq. (31), becomes $T^i=T_0^i+\epsilon h_1 T_1^i$, where $T_0^i(x)=KT_0/(K+h_0)$ and $T_1^i(x)=-KT_0/(K+h_0)^2$. Equation (41) is solved subject to the boundary condition

$$h_1 \text{ bounded as } x\to\pm\infty. \tag{43}$$

When discretized in space using fourth-order, centered finite differences, Eqs. (41) and (43) yield a linear system of equations that can be written in vector form as

$$\frac{\partial \boldsymbol{h}_1}{\partial t}=\mathbf{A}\boldsymbol{h}_1, \tag{44}$$

where $\mathbf{A}$ is a linear autonomous matrix and $\boldsymbol{h}_1$ is the discretized form of h_1. Assuming exponential time dependence for h_1, $h_1(x,t)=h_1(x)\exp(\beta t)$, yields the eigenvalue problem $\beta\boldsymbol{h}_1=\mathbf{A}\boldsymbol{h}_1$. For each value of the wave number q, the n eigenvalues of the matrix $\mathbf{A}$, $\beta_n(q)$, were found using the MATLAB 6.1 function eig. The eigenvalues plotted in Figs. 5 and 6 below, which correspond to the discrete modes and the lead-

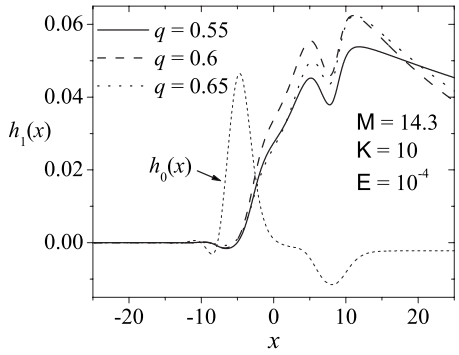

FIG. 4. Shape of discrete modes for a linearly stable film. The eigenfunctions are normalized such that $\int_{x=-40}^{x=40}|h_1|^2dx=1$. The (rescaled) base profile $h_0(x)$ is superimposed for reference.

ing mode from the continuous spectrum, are insensitive to the order of square matrix **A**, which is of dimension 2000 or larger for all computations.

The operator $\mathbb{L}\equiv\Sigma\mathbb{L}_i$ can have both a discrete and a continuous spectrum in the x direction. The discrete spectrum is comprised of decaying eigenfunctions such that $h_1(x\rightarrow\pm\infty)\rightarrow 0$, which correspond to perturbations localized around the spatial variations of the base state that are associated with instability. The continuous spectrum is comprised of eigenfunctions that exhibit bounded, oscillatory behavior as $x\rightarrow\pm\infty$ and can be associated with perturbations to the flat-film regions away from the heater, and these modes are always stable. For a flat film of unit thickness, the spectrum of eigenfunctions that approach bounded oscillations as $x\rightarrow\pm\infty$ consists of Fourier modes, $h_1\sim\exp(\beta t+i\kappa x+iqy)$. In the present case, $T_{0x}\rightarrow 0$, and $h_0\rightarrow 1$ as $x\rightarrow-\infty$ and $h_0\rightarrow c_1$ as $x\rightarrow+\infty$. Away from the temperature gradient, the continuous modes will therefore have a similar structure to those for a flat film. The locus of the essential spectrum for a given q can be found by substituting $h_1(x,y,t)=\exp(\beta t+i\kappa x+iqy)$ into Eq. (41) as $x\rightarrow\pm\infty$, which yields

$$\beta=-(q^2+\kappa^2)^2-3i\kappa,\quad \kappa\in(-\infty,+\infty). \tag{45}$$

The mode with the smallest decay rate corresponds to $\kappa=0$, and the leading eigenvalue with the largest real part from the continuous spectrum is therefore given by $\beta=-q^4$. The corresponding eigenfunction approaches constant values away from the heater, $h_1\rightarrow c_\pm$ as $x\rightarrow\pm\infty$, and this mode is easily found with the boundary conditions h_{1x}, $h_{1xxx}\rightarrow 0$ as $x\rightarrow\pm\infty$. Other modes with $\kappa\neq 0$ can be found by using a global Fourier spectral expansion in the x coordinate.[24]

In addition to this stable, continuous spectrum, a band of stable, discrete modes appears above a critical Marangoni parameter $M_c=M_c(K,E)$ for volatile films. The corresponding eigenfunctions are peaked near the depression at the downstream edge of the heater and decay to zero very slowly as $x\rightarrow\infty$, as shown in Fig. 4. These discrete modes are associated with a transverse thermocapillary flow and were not found for a linearly stable, nonvolatile film.[26] If M is increased from M_c, there is a second, critical Marangoni parameter $M^r_{\rm crit}$ above which a portion of the discrete band becomes unstable, corresponding to the formation of rivulets

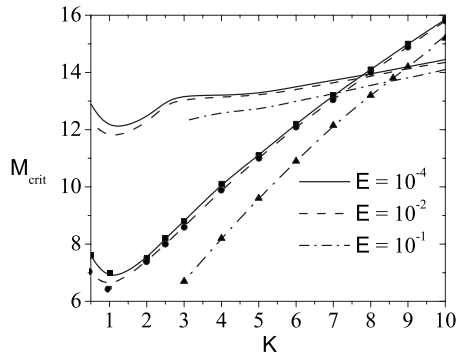

(a)

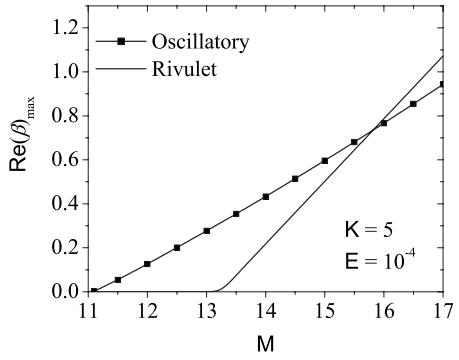

(b)

FIG. 5. (a) Critical Marangoni parameter ($M_{\rm crit}$) vs K corresponding to the two types of instabilities for different values of E. The curves with symbols correspond to the thermocapillary instability with complex eigenvalues. (b) Maximum $\Re e(\beta)$ vs M for $K=5$ and $E=10^{-4}$. At $M=13.25$, unstable discrete modes appear, corresponding to a rivulet instability.

at the downstream edge of the capillary ridge (upstream edge of the heater). The values of M_c and $M^r_{\rm crit}$ are typically close together. For example, for $K=10$ and $E=10^{-4}$, $M_c=13.8$ and $M^r_{\rm crit}=14.3$.

For a highly volatile liquid, the large heat loss from evaporation can lead to two different types of instabilities. In addition to the rivulet instability for $M>M^r_{\rm crit}$, a band of small transverse wave numbers q corresponds to unstable, complex eigenvalues for $M>M^t_{\rm crit}$. The eigenfunctions are associated with an oscillatory, thermocapillary long-wave instability above the heater in the streamwise direction, and these discrete modes are not found unless $M>M^t_{\rm crit}$ (i.e., there is no such discrete band that is entirely stable). The critical Marangoni parameters $M^r_{\rm crit}$ and $M^t_{\rm crit}$ above which the rivulet and thermocapillary instabilities, respectively, develop for various E and K are shown in Fig. 5(a).

For smaller K, corresponding to increased volatility and more heat transfer from the film, $M^t_{\rm crit}<M^r_{\rm crit}$ because of a substantial streamwise thermocapillary flow induced by the variation of h_1 above the heater where $T_0\approx 1$. This nonuniform film thickness leads to variations in T^i and Marangoni stresses (thicker regions are cooler and have larger surface tension) that compete with gravity to yield the oscillatory instability. For larger K, $M^r_{\rm crit}<M^t_{\rm crit}$ because the Marangoni stresses that drive the thermocapillary instability above the heater are reduced by the smaller heat flux from the film by evaporation, while the rivulet instability develops once the

capillary ridge is sufficiently large (even without heat loss from the film). Although $M_c < M^r_{\text{crit}}$, the relationship between M_c and M^t_{crit} depends on the values of K and E. Evaporation is found to be destabilizing, as an increase in E decreases both M^r_{crit} and M^t_{crit}, with the decrease in the critical Marangoni parameter more pronounced for the thermocapillary instability and for smaller K (more volatile liquids). There is a crossover value of K corresponding to the onset of both types of instabilities at M_{crit}. For example, for $E=0.1$, $K_{\text{cross}} \approx 8.57$ at which $M_{\text{crit}} \approx 13.7$. The dependence of M_{crit} on K is nonmonotonic, with a minimum occurring at $K_{\text{min}} \approx 1$ for both types of instability. Because $T^i \approx 0$ as $K \to 0$, $h(x,y) \approx 1$ and thermocapillary effects are small, so the film becomes stable to both the rivulet and thermocapillary instabilities.

Plotted in Fig. 5(b) are the real parts of the largest eigenvalues, $\max_q[\Re e(\beta)]$, versus M for constant E and K for the rivulet and thermocapillary instabilities. For $M < 13.28$, the only unstable modes are complex. For $13.28 < M < 15.8$, both real and complex modes are unstable, and the oscillatory, thermocapillary mode of instability dominates. Although $M^t_{\text{crit}} < M^r_{\text{crit}}$ for $K=5$ and $E=10^{-4}$, the rivulet instability dominates for $M \geq 15.8$ because the capillary ridge is sufficiently large to favor rivulet formation. By contrast, the thermocapillary instability occurs because of ∇T^i above the heater upon imposition of a perturbation h_1 (which makes the film thickness and hence T^i vary spatially) and not on the capillary ridge, as discussed further in Sec. III D.

The effect of the evaporative mass flux and heat transfer on the linear stability of the flowing film is shown in Fig. 6. A nonvolatile liquid, $K \to \infty$, is stable to transverse perturbations for $M=15$,[26] and the dispersion curve $\beta(q)$ follows the continuous spectrum with $\kappa=0$: $\beta=-q^4$. For a volatile liquid corresponding to $K=10$, the film becomes more unstable as the evaporative mass flux E increases, as seen from Fig. 6(a). The stable band of discrete modes, which is plotted for $M=14.3$, is absent for a film of nonvolatile liquid.[26]

Shown in Fig. 6(b) are the dispersion curves for the rivulet and thermocapillary instabilities for $M=15$, $K=5$, and $E=10^{-4}$. For smaller q, the unstable modes are temporally oscillatory due to complex eigenvalues with positive real parts. As q is increased, the growth rate of the complex mode decreases, and the discrete modes corresponding to rivulet formation become unstable at $q \approx 0.56$. At $q \approx 0.5966$, $\beta_{\text{riv}} = 0.0472$ and $\beta_{\text{oscil}} = 0.0472 \pm 2.031i$, and this is a repeated eigenvalue with two different eigenfunctions corresponding to the two different types of instability.

Shown in Fig. 6(c) are the dispersion curves for $M=15$ and $E=0.1$ for liquids of different volatilities (different K). The growth rates of both types of instability increase with decreasing K. The thermocapillary instability at small q is absent for $K=10$ but develops for $K=9$. The leading eigenvalue follows several different branches of the dispersion curve as q varies. For example, for $K=9$, the thermocapillary instability develops for $0 \leq q < 0.24$. The eigenvalue follows the stable, continuous spectrum for $0.25 \leq q \leq 0.48$, stable discrete modes for $0.485 \leq q < 0.493$, unstable discrete modes (rivulet instability) for $0.494 \leq q < 0.74$, stable discrete modes for $0.75 \leq q < 0.88$, and the continuous spectrum for $q \geq 0.89$.

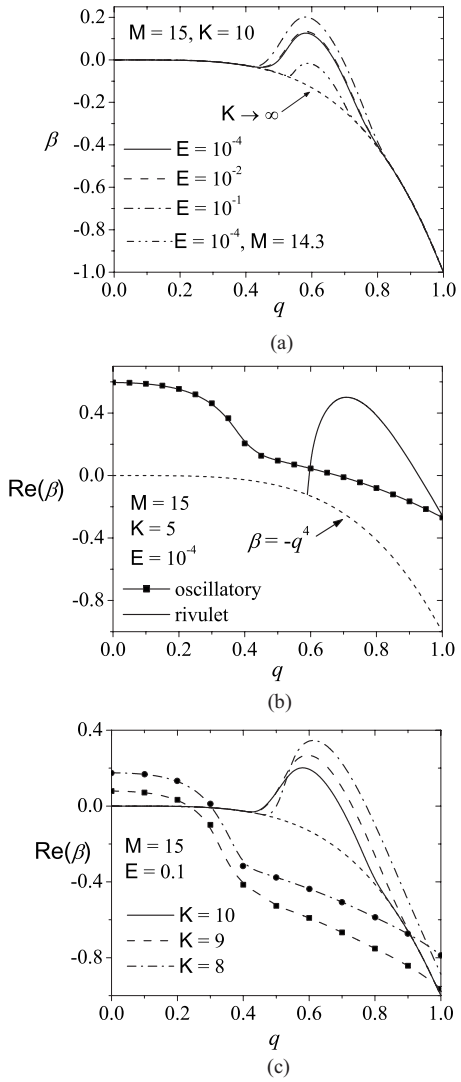

FIG. 6. (a) Effect of evaporation on the dispersion curves. For a nonvolatile liquid ($K \to \infty$), the film is stable for $M=15$. (b) Dispersion curves corresponding to the thermocapillary and rivulet instabilities. (c) Dispersion curves for different K.

Eigenfunctions corresponding to the dispersion curve shown in Fig. 6(c) for $M=15$, $K=8$, and $E=0.1$ are plotted in Fig. 7. At $q=0$, the growing mode is complex. The oscillations are most pronounced over the heater, where the film has the highest interfacial temperature T^i. Evaporation is most pronounced in this region, leading to a large evaporative heat flux above the heater. Variations in h_1 in this region therefore lead to significant Marangoni stresses through their influence on T^i_{1x}, and the competition between these stresses and gravity leads to the oscillatory behavior in this region. The oscillations decay downstream of the heater by $x \approx 40$. The leading stable, continuous mode for $q=0.35$ is plotted, which shows that $h_1 \to c_{\pm}$ as $x \to \pm\infty$. For $q=0.6$, the leading mode is unstable and discrete and is associated with the rivulet instability that develops at the downstream portion of the capillary ridge. The discrete, stable mode for $q=0.8$ attains

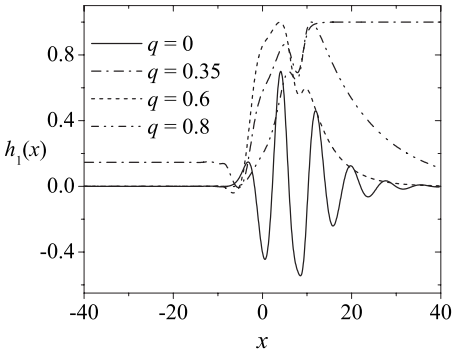

FIG. 7. Eigenfunctions for different q corresponding to dispersion curve for $M=15$, $K=8$, and $E=0.1$ in Fig. 6(c). The eigenfunctions are normalized such that $\int_{x=-40}^{x=40}|h_1|^2dx=1$.

its maximum at the downstream of the capillary ridge and slowly decays as $x\to\infty$. The discrete modes associated with rivulet formation in this linearly unstable film are focused at the forward portion of the capillary ridge, making them qualitatively different from the discrete modes for a linearly stable film, as plotted in Fig. 4. In addition, the discrete modes for linearly unstable films decay more quickly as $x\to\infty$ than the corresponding modes for linearly stable films.

The difference between the two types of instabilities can be visualized by superimposing the eigenfunctions on the base states. Shown in Fig. 8 are wireframe plots of $h(x,y,t)=h_0(x)+\epsilon h_1(x)\cos(qy)$ for $M=15$, $E=0.1$, and $K=8$. In Fig. 8(a), the oscillatory, thermocapillary instability for $q=0$ can be seen downstream of the capillary ridge, as the film is uniform in the y direction. The oscillations arise from the competition between flow due to gravity and the (streamwise) thermocapillary flow induced by perturbations to the film above the heater (due to T^i_{1x}). Shown in Fig. 8(b) is $h(x,y,t)$ for $q=0.1$. The film profile is more complicated because periodicity in the y direction is added to the streamwise variation apparent in Fig. 8(a), and the perturbations appear slanted in the x-y plane. The rivulet instability for $q=0.6$ is shown in Fig. 8(c) and is qualitatively different from the thermocapillary instability shown above. These periodic rivulets are localized at the downstream portion of the capillary ridge, where the Marangoni stress at the upstream edge of the heater opposes the bulk flow. This instability is enhanced by the transverse thermocapillary flow above the heater (due to perturbation variations in the y direction) but occurs even in the limit $K\to\infty$, in which case variations in the film thickness do not induce Marangoni stresses $[T^i(x,y)\to T_0(x)]$.

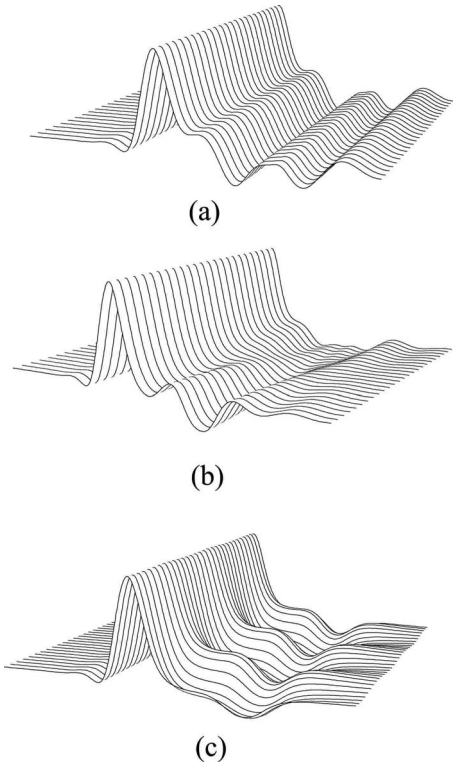

FIG. 8. Wireframe plots of $h(x,y,t)=h_0(x)+\epsilon h_1(x)\cos(qy)$ for $M=15$, $E=0.1$, and $K=8$ for (a) $q=0$ (thermocapillary), (b) $q=0.1$ (thermocapillary), and (c) $q=0.6$ (rivulet).

C. Effect of temperature profile

For a nonvolatile liquid with $\mathrm{Bi}\to 0$, Tiwari and Davis[26] found that the width (streamwise extent) of the heater has essentially no influence on the stability of the film. As the temperature increase at the heater becomes steeper, corresponding to an increase in the parameter ω, they found that M^r_{crit} monotonically decreases until saturating for $\omega\geq 5$. For the volatile liquids considered here, both the steepness and width of the heater alter the stability results. The temperature of the substrate is modeled as in Eq. (40), and ω and χ are varied for this analysis. Shown in Fig. 9(a) are the base-state profiles for different values of the steepness parameter ω for a heater of fixed width with $\chi=4$. The capillary ridge increases in magnitude and steepens as ω increases but asymptotes for $\omega\geq 5$. The shape of the film above the downstream edge of the heater is not affected by changes in these parameters. The film is unstable for $\omega=2$ but stable for the other profiles shown. The critical Marangoni number at rivulet formation, M^r_{crit}, is plotted as a function of ω in Fig. 9(b) for several different ω and χ. For $\chi=8$, M^r_{crit} is nonmonotonic, decreasing from $\omega=1$ to $\omega=2$ and then increasing as ω is increased further. The corresponding curve for $\chi=4$ is qualitatively similar but does not vary as strongly with ω. Wider heaters correspond to slightly more stable films, although the influence of the heater width on M^r_{crit} is not observed for a nonvolatile liquid, which corresponds to the limit $K\to\infty$.

In addition, M^r_{crit} is plotted versus ω in Fig. 9(b) for different combinations of K and E for $\omega\chi=4$ to illustrate the combined effects of heater width and steepness. For each set of parameters, M_{crit} exhibits a pronounced minimum for $\omega=3.5$ and a maximum for $\omega\approx 5$. The rivulet instability occurs from the interaction of gravity, capillary flow, evaporation, and streamwise and transverse thermocapillary flows, and these mechanisms are nonlinearly coupled through the base state, which gives rise to the strong variation in M^r_{crit} for different temperature profiles. As shown in Fig. 9(c), the base profiles corresponding to the onset of instability at M^r_{crit} can differ drastically as ω and χ vary, and stability cannot be inferred from the shape of the film. An energy analysis of **A**

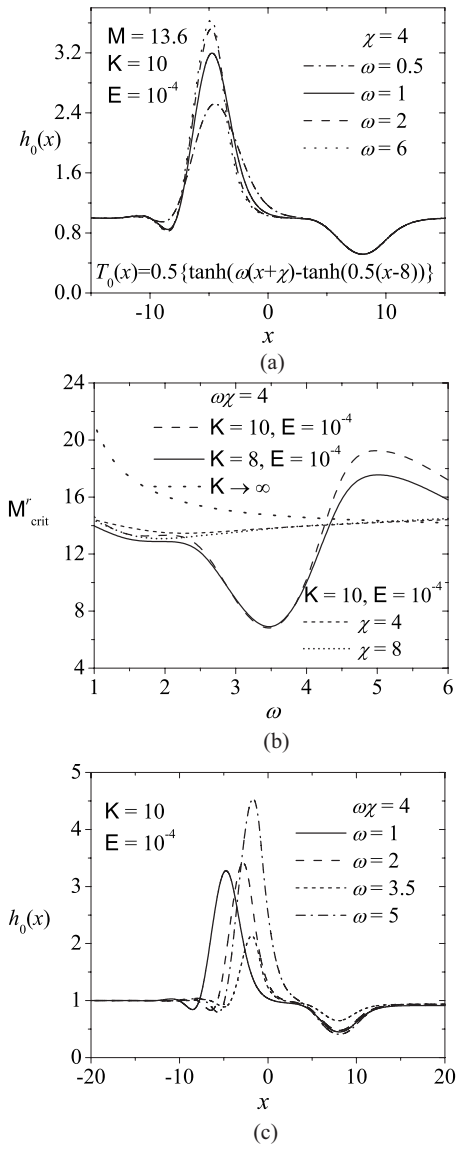

FIG. 9. (a) Effect of the steepness parameter ω on the film profile when the width is fixed with $\chi=4$. Profiles for $\omega=0.5$,1, and 6 are stable, whereas $\omega=2$ is unstable. (b) Critical Marangoni parameter M^r_{crit} vs ω. (c) Representative base profiles at M^r_{crit}, corresponding to instability onset.

is presented in Sec. III D to provide further insight into the different mechanisms that drive the linear instability.

D. Energy analysis

The exponential growth rate β of perturbations can be interpreted as an energy production rate $\dot{E}$,[44] and the contributions of the individual terms in the disturbance operator $\mathbb{L}$ to $\dot{E}$ can be isolated to infer the influence of various physical mechanisms on the instability. The terms in Eq. (41) make contributions $\dot{E}_n$ to $\dot{E}$, which can be found from[44]

$$\dot{E}_n = \frac{\langle h_1, \mathcal{L}_n h_1 \rangle}{\langle h_1, h_1 \rangle}, \tag{46}$$

where $\langle \cdot, \cdot \rangle$ denotes the inner product associated with the L^2 norm. Each $\mathcal{L}_n$ is a group of terms from $\mathbb{L}$ listed in Table II along with its physical meaning. These terms depend nonlinearly on the base flow solution, $h_0(x)$, and perturbation wave number q. Terms corresponding to $\dot{E}_n<0$ are stabilizing, while terms corresponding to $\dot{E}_n>0$ are destabilizing. Noting that $\mathbb{L}=\Sigma\mathcal{L}_n$, it follows directly from Eq. (46) that $\Sigma\dot{E}_n=\beta$.

Shown in Fig. 10(a) is a plot of $\dot{E}_n$ versus q for $M=15$, $K=10$, and $E=0.1$ for which the film is susceptible to a rivulet instability but not an oscillatory, thermocapillary instability. For this volatile liquid, the dominant mechanism leading to the rivulet instability is term 9, which corresponds to thermocapillary flow in the y direction due to transverse temperature gradients induced by the perturbation. (For $K\to\infty$, by contrast, this flow is absent, and the instability is dominated by terms 3 and 4.[23,26]) Flow in the x direction due to gravity (term 3) is also strongly destabilizing for $q\approx0.6$. Other significant destabilization is due to capillary flow driven by the base-state capillary pressure gradient acting on the perturbation (term 4) and thermocapillary flow in the x direction due to streamwise temperature variations induced by the perturbation (term 8). Term 8 arises due to variations in the interfacial temperature ($T^i=T^i_0+\epsilon h_1 T^i_1$) induced by perturbations to the film thickness (h_1) and vanishes in the limit $K\to\infty$, which corresponds to no heat transfer from the free surface and $T^i=T_0$. The dominant stabilizing contribution is provided by term 7, which corresponds to thermocapillary flow in the x direction due to the Marangoni stress from T^i_{0x} acting on variations in the perturbation thickness. This stress provides a restoring flow to perturbations to the capillary ridge reminiscent of stabilization by substrate topography[31] (which is due to a capillary pressure gradient). Additional stabilizing contributions are made by terms 1, 2, and 6. The influence of evaporation on the perturbation (term 10) is essentially neutral, but the effect of evaporation is more pronounced through its influence on the base state, through which it is nonlinearly coupled to capillary pressure gradients, gravity, and the Marangoni stress.

Plotted in Fig. 10(b) are $\dot{E}_n$ versus q for $M=15$, $K=8$, and $E=0.1$. For these parameters, the film is susceptible to an oscillatory, thermocapillary instability for $0<q<0.32$ and a rivulet instability for $0.53<q<0.78$. Only the real parts of $\dot{E}_n$ are plotted. These results indicate that this thermocapillary instability is primarily due to term 8, with term 3 (gravity) making an additional destabilizing contribution. The dominant stabilization is provided by term 1, and term 7 is also stabilizing. The rivulet instability for $0.5<q<0.8$ is interpreted as for Fig. 10(a). The imaginary parts of $\dot{E}_n$ corresponding to Fig. 10(b) are plotted versus q in Fig. 10(c). The oscillatory component of the thermocapillary instability is due primarily to terms 3 (gravity), which acts in the $+x$ direction, and 7 (thermocapillary flow in the streamwise direction due to the Marangoni stress from T^i_{0x} acting on the perturbation), which acts in the $-x$ direction. Plotted in Fig. 10(d) are $\dot{E}_n$ versus K for $M=15$, $E=0.1$, and $q=q_{\max}$, which is the wave number corresponding to $\beta_{\max}$, the eigenvalue with the largest real part for each set of parameters. An abrupt switch in the dominant instability mechanism is apparent and corresponds to the switch from a thermocapillary instability for $K<5.63$ to a rivulet instability for $K\geq5.63$.

TABLE II. Terms contributing to the energy production rate of perturbations to the film and their physical interpretation.

Term	Expression	Physical meaning
1	$-(h_0^3 h_{1xxx})_x$	Capillary flow in the x direction induced by perturbation curvature variation in x
2	$q^2(h_0^3 h_{1x})_x$	Capillary flow in the x direction due to streamwise change in transverse perturbation curvature
3	$-3(h_0^2 h_1)_x$	Flow in the x direction due to gravity
4	$(-3h_0^2 h_{0xxx} h_1)_x$	Capillary flow in the x direction driven by the base-state capillary pressure gradient acting on perturbation
5	$q^2 h_0^3 h_{1xx}$	Capillary flow in the y direction induced by perturbation curvature in x
6	$-q^4 h_0^3 h_1$	Capillary flow in the y direction induced by perturbation curvature in y
7	$M(T_{0x}^i h_0 h_1)_x$	Thermocapillary flow in the x direction due to unperturbed Marangoni stress acting on perturbation
8	$M[h_0^2(T_1^i h_1)_x]_x$	Thermocapillary flow in the x direction due to streamwise temperature gradient induced by perturbation thickness variation in x
9	$-q^2 M h_0^2 T_1^i h_1$	Thermocapillary flow in the y direction due to transverse temperature gradient induced by perturbation thickness variation in y
10	$[ET_0/(K+h_0)^2]h_1$	Evaporative flow due to perturbation

It was shown in Sec. III C that the steepness of the temperature profile has a nonmonotonic effect on M_{crit}^r. Plotted in Fig. 11(a) are results of an energy analysis for $M=6$, $K=10$, and $E=10^{-4}$ with $\omega=3.5$ and $\omega\chi=4$. As seen from Fig. 9(c), this unstable film has a relatively small capillary ridge, with $\max(h_0)\approx 2$. This film undergoes a typical rivulet instability, with terms 4 and 3 the most destabilizing, and terms 8 and 9 providing additional but small destabilization. The most significant stabilizing contributions are made by terms 7, 1, 6, and 2. For a steeper temperature increase ($\omega=5$) and all other parameters fixed, however, the film is linearly stable. The energy analysis results plotted in Fig. 11(b) indicate that while term 4 is still most destabilizing, term 7 is also destabilizing. This term, which corresponds to streamwise thermocapillary flow due to T_{0x}^i acting on the perturbation, was always stabilizing in previous energy analysis results presented here and in earlier work.[23,26] Furthermore, term 3 (gravity), which was destabilizing in all previous results, is now stabilizing. This interesting behavior is due to the precise positioning of the capillary ridge relative to the steep temperature gradient at the upstream edge of the heater.

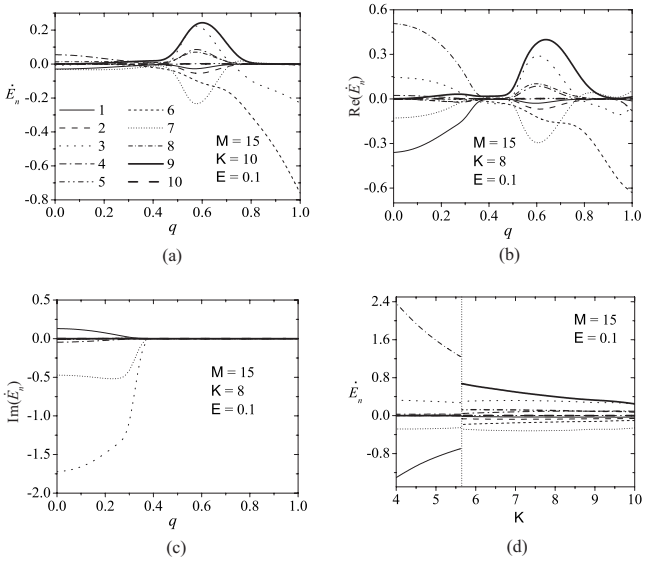

FIG. 10. Energy analysis results. (a) $\dot{E}_n$ vs q for $M=15$, $K=10$, and $E=0.1$. (b) $\Re\mathrm{e}(\dot{E}_n)$ vs q for $M=15$, $K=8$, and $E=0.1$. (c) $\Im\mathrm{m}(\dot{E}_n)$ vs q for $M=15$, $K=8$. and $E=0.1$. (d) $\dot{E}_n$ vs K for $M=15$ and $E=0.1$ for $q=q_{\max}$. The vertical dotted line delineates the rivulet instability (larger K) from the thermocapillary instability (smaller K).

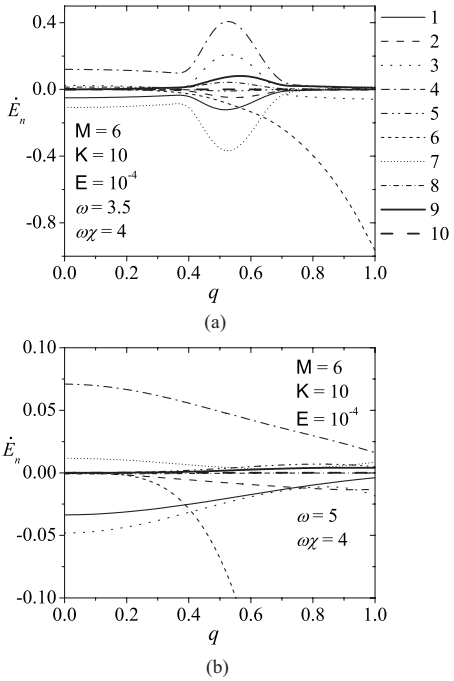

FIG. 11. Energy analysis results for $M=6$, $K=10$, and $E=10^{-4}$ for (a) $\omega=3.5$ (undergoes rivulet instability) and (b) $\omega=5$ (linearly stable).

IV. DISCUSSION

A. Film profile

As shown in Fig. 9(a), with heat transfer from the liquid film to the surrounding gas, the film profile is sensitive to the exact temperature profile imposed on the substrate, $T_0(x)$, which is not known for most relevant experimental data, making direct comparisons to experiment difficult. With a suitable choice of temperature profile, however, the base states $h_0(x)$ computed from Eq. (37) have the same quantitative agreement with experimental data as the profiles computed by Skotheim *et al.*,[23] who derived the analogous lubrication model for the case of a nonvolatile film. The lubrication approximation breaks down when the aspect ratio $\hat{h}_\infty/l_c$ is no longer small, which is the case for some of the thicker films investigated in experiments[27,28,45] ($\hat{h}_\infty \approx 100$ μm), as noted by Skotheim *et al.*[23] Furthermore, for thicker films, inertia may also become important. Including the first-order inertial term as in the Benney equation[15,46] adds a term $Q(h^6h_x)_x$ to Eq. (37), where $Q=6/5\,\mathrm{Re}(3\mathrm{Ca})^{1/3}$, with $\mathrm{Re}\equiv g\hat{h}_\infty^3/(3\nu^2)$ the Reynolds number. Computations with Eq. (37) for $Q<0.04$ (corresponding to a water film up to approximately 50 μm thick) reveal a small influence of inertia on the base states and linear stability predictions for the rivulet instability. Consequently, film profiles computed using Eq. (37) share the same strong agreement with experimental measurements as those computed by Scheid *et al.*[16] for the same choice of temperature profile for the range of their parameter $\mathrm{R}\equiv 3\mathrm{Re}\leq 1.5$.

As noted by Kalliadasis *et al.*,[10] in the limit of small inertia and for a nearly vertical substrate, the behavior of the free surface depends only on a single combined parameter and is universal for all Re. For the present case, the behavior is universal for all Re and Ca provided that $Q\to 0$ and depends only on the parameter M. Noting that $\mathrm{Ca}=\mathrm{Re}^{2/3}/(3^{1/3}\mathrm{Ka})$, where $\mathrm{Ka}\equiv\sigma_0/(\rho\nu^{4/3}g^{1/3})$ is the Kapitza number that depends only on the physical properties of the liquid, reveals that the behavior of the interface depends only on M and is universal for all Ka and Re consistent with this limit. This behavior explains the strong agreement with experimental profiles reported by both Scheid *et al.*[16] (who included inertia) and Skotheim *et al.*[23] (who neglected inertia). For a volatile film, E is an additional parameter that influences the film dynamics.

B. Rivulet instability

For the rivulet instability, because of the weak dependence of the dimensionless instability wave number on M, this analysis predicts that the wavelength of the rivulet instability scales as $\lambda_{\max}=(2\pi/q_{\max})l_c\propto\sigma_0^{1/3}$. This scaling is in very good agreement with the result $\lambda_{\max}\propto\sigma_0^{0.365}$ from experiments and direct numerical simulation of the full Navier–Stokes and energy equations by Frank and Kabov.[25] Furthermore, just as for the analysis by Tiwari and Davis[26] for $\mathrm{Bi}=0$, the predictions of rivulet instability above a critical Marangoni number for a finite band of wave numbers separated from zero and the marginal stability curves are consistent with the results of Frank and Kabov,[25] although differences in the temperature at the solid substrate and values of the dimensionless parameters preclude an exact comparison. An important difference from the study of Tiwari and Davis[26] is that for the present model, in which heat transfer from the liquid film to the surrounding gas (from evaporation or convection) is significant, the height of the capillary ridge at the onset of instability can be significantly smaller than the rather large values found in Ref. 26 for $\mathrm{Bi}\to 0$. For example, $\hat{h}_{\max}/\hat{h}_\infty\approx 2$ for $\omega=3.5$ in Fig. 9(c), which is closer to the values found in experiments[16,17,45,47] even for the model temperature profile used in this study that differs from the one in experiments.

Skotheim *et al.*[23] also compared their linear stability predictions to experimental results. While their predicted instability wave number was consistent, their predicted critical Marangoni number at instability onset was about five times larger than the "experimental" value. Because the surface temperature in the experiments is not known, they determined the experimental Marangoni number (and other parameters in their model) by computing the film profile for different values of the Marangoni number until the maximum film thickness matched the experimentally measured maximum height. In the variables of the present work, these values correspond to $M\approx 2.7$–3.0. From Fig. 9(b), $M_{\mathrm{crit}}\approx 6.5$ for the profile with $\omega=3.5$, which is about 2.5 times too large. Given the uncertainty in the experimental temperature profile and the value of Bi, however, this agreement is reasonable, especially given the strong dependence of the stability results on the specific temperature profile, as reported in this work. Furthermore, the water-ethanol mixture used in the experiments may give rise to solutal Marangoni effects or complications from nonuniform evaporation of the mixture, neither of which are considered in the theoretical model.

C. Thermocapillary instability

For a nonvolatile liquid film falling along a homogeneously heated surface, the leading-order, long-wave equation that replaces Eq. (37) in two dimensions is[8,15]

$$\frac{\partial h}{\partial t}+Q(h^6h_x)_x+\left[(1+h_{xxx})h^3+\frac{MKh^2h_x}{(K+h)^2}\right]_x=0, \tag{47}$$

where $K=\mathrm{Bi}^{-1}$. Letting $h(x,t)=1+\epsilon\exp[ikx+(\beta_{\mathrm{Re}}+i\beta_{\mathrm{Im}})t]$, a linear stability analysis of Eq. (47) yields an expression for the instability growth rate,

$$\beta_{\mathrm{Re}}=k^2Q+\frac{MK}{(K+1)^2}k^2-k^4. \tag{48}$$

The most unstable wave number is

$$k_{\max}=\left(\frac{MK}{2(K+1)^2}+\frac{Q}{2}\right)^{1/2}. \tag{49}$$

For $Q=0$, $M=15$, and $K=8$, $\lambda_{\max}=2\pi/k_{\max}\approx 7.3$, which is very close to the wavelength of the thermocapillary instability for flow over a localized heater ($\lambda_{\max}\approx 8.1$), as found from the leading eigenfunction for $q=0$ in Fig. 7, even though the finite length of the heater and the deformation of the film from Marangoni stresses at the heater edges affect

the wavelength of the oscillations. This thermocapillary instability disappears if the width of the heater becomes sufficiently small. Based on the linear stability results for a uniformly heated surface in Eq. (48), the critical wave number above which the film is stable is given by $k_{crit}^2=Q+MK/(K+1)^2$. For the finite heater, the edge effects also influence k_{crit}. It was found that the thermocapillary instability does not exist for a heater of width $w\leq 2$ for the range of parameter values considered in this work. This dependence of the oscillatory thermocapillary instability on the width of the heater explains why this mode of instability was not found by Kalliadasis *et al.*[24] even though they used the relatively large value of Bi=1 for their computations.

For the thin films considered here, inertia would have only a small influence on the instability wavelength. For example, for $Q=0.04$, λ_{max} would change to 7.2 dimensionless units for a homogeneously heated surface. For a surface without heating, the wavelength of the inertial surface-wave instability is predicted to be $\lambda_{max}\approx 44$ for $Q=0.04$, indicating that the thermocapillary instability predicted here for sufficiently large heat transfer rates would be clearly distinguished from the surface-wave instability in experiments by the vastly different wavelengths at instability onset. The interaction of inertial terms with the thermocapillary instability for a locally heated film, including the nonlinear film evolution and potential secondary instability of periodic states that develop from saturation of the oscillatory instability, is an interesting topic for future study. Preliminary computations indicate that, for the range of K corresponding to strong thermocapillary effects from film deformation above the heater [where $T_0(x)\approx 1$], this oscillatory instability mode is enhanced for $Q\geq 0.04$ due to the influence of inertia on the deformed film. Finally, as $K\rightarrow 0$, $h_0(x)\rightarrow 1$, as shown in Fig. 2(a) because the interfacial temperature becomes uniform despite the nonuniformly heated substrate. In this limit both the rivulet and thermocapillary instabilities disappear, which is advantageous for many applications because the film may rupture after instability onset, creating dry regions that diminish heat transfer. Specialty coolants such as FC-72 and FC-77 have such small values of K, making them well suited for heat transfer in small-scale applications.

V. CONCLUSION

The stability of a volatile liquid film flowing over a locally heated surface was examined using a lubrication analysis. The Marangoni stress at the upstream edge of the heater opposes the bulk flow and induces the formation of a pronounced capillary ridge. At the downstream edge of the heater, the Marangoni stress is aligned with the bulk flow and induces a trough. The effect of evaporation is taken into account through a model with two dimensionless groups. The parameter K quantifies the vapor pressure driving force for mass transfer from the liquid-gas interface and behaves as an inverse Biot number because of the coupling of heat transfer to evaporation of the liquid. In the limit of no evaporation, this analogy is exact, as $K=\mathrm{Bi}^{-1}$. The parameter E is the ratio of the convective to evaporative time scales. Evaporation was shown to have a significant effect on the dynamics and stability of the film, with the base profiles determined from a nonlinear coupling between the Marangoni stress, capillary pressure gradients, evaporation, and gravity. The steady profiles corresponding to a continuous film cannot be found due to rupture at the trough for small values of K, corresponding to a highly volatile liquid, and moderate values of E, corresponding to a large heat flux at the heater.

For weaker evaporation, the stability of the two-dimensional base states to transverse perturbations was investigated. The linear operator that governs the evolution of small perturbations to the film has both a discrete and a continuous spectrum. The continuous modes are stable for spanwise perturbations of any wave number and consist of eigenfunctions that approach bounded oscillations at the infinities. Although their shape is modified by the capillary ridge near the heater, their corresponding spectrum is described by the dispersion relation of a flat film. As the Marangoni parameter is increased beyond a critical value, the discrete spectrum appears for a finite band of transverse wave numbers separated from zero. The discrete modes are localized at the capillary ridge. A band of stable discrete modes is present for the volatile liquid film but was not seen for a nonvolatile film with vanishing Biot number.[26] As the Marangoni parameter is increased further, beyond a second critical value, a band of unstable discrete modes appears that is associated with the formation of rivulets aligned with the flow and periodic in the spanwise direction. These critical Marangoni parameters decrease as K is decreased, corresponding to a more volatile liquid. Evaporation due to high volatility of the liquid is therefore destabilizing toward rivulet instability because it increases the transverse Marangoni stress at the free surface due to perturbations to the film. As the liquid volatility is increased, another band of discrete modes is found, which is associated with an oscillatory, thermocapillary instability above the heater. This band is entirely absent for a nonvolatile liquid with small Biot number. The eigenfunctions corresponding to the rivulet instability have maxima at the forward portion of the capillary ridge induced by the heater, while the eigenfunctions corresponding to the oscillatory instability are most pronounced over the heater and decay downstream. The critical Marangoni parameters corresponding to the two types of instabilities for different evaporation conditions were computed and plotted. The destabilizing influence of increasing E was shown to be more significant for a more volatile liquid (small K).

An energy analysis of the governing linear operator was performed to determine the effect of evaporation on the linear stability of the base profiles. It was found that for a volatile liquid, transverse variations in the interfacial temperature created by a perturbation to the film thickness cause a thermocapillary flow in the y direction that leads to a rivulet instability. By contrast, when evaporation is absent, capillary flow in the streamwise direction due to the perturbation was the leading instability mechanism. The dominant mechanism leading to the oscillatory, thermocapillary instability was found to be thermocapillary flow in the streamwise direction due to streamwise variations in the interfacial temperature, which are induced by perturbations to the film thickness in the presence of significant heat transfer from the

free surface by evaporation. It was also shown that the competition between gravity and the Marangoni stress from the unperturbed temperature profile leads to the temporal oscillations associated with this instability.

The steepness of the temperature gradient at the solid surface was varied and found to have a nonmonotonic effect on the critical Marangoni parameter for the volatile liquid film, in contrast to the monotonic decrease in critical Marangoni parameter for a nonvolatile liquid film.[26] The base profiles for the film when plotted at the critical conditions for different values of the steepness parameter showed a significant variation in the amplitude of the capillary ridge. It was found from the energy analysis that the stabilizing and destabilizing roles of gravity and thermocapillary stress are interchanged as the steepness of the temperature profile and heater width were varied due to the specific positioning of the capillary ridge relative to the heater. This sensitivity of the stability results to the specific temperature profile reflects the nonlinear coupling of gravity, capillary pressure gradients, Marangoni stresses, and evaporation through the base states and is responsible for the nonmonotonic dependence of the critical Marangoni parameter at instability onset.

ACKNOWLEDGMENTS

J.M.D. kindly acknowledges support from NSF Award No. CBET-0644777 and the Camille Dreyfus Teacher-Scholar Awards Program.

[1] A. Oron, S. H. Davis, and S. G. Bankoff, "Long-scale evolution of thin liquid films," Rev. Mod. Phys. **69**, 931 (1997).
[2] S. H. Davis, "Thermocapillary instabilities," Annu. Rev. Fluid Mech. **19**, 403 (1987).
[3] M. F. Schatz and G. P. Neitzel, "Experiments on thermocapillary instabilities," Annu. Rev. Fluid Mech. **33**, 93 (2001).
[4] J. P. Burelbach, S. G. Bankoff, and S. H. Davis, "Nonlinear stability of evaporating/condensing liquid films," J. Fluid Mech. **195**, 463 (1988).
[5] E. Sultan, A. Boudaoud, and M. B. Amar, "Evaporation of thin film: Diffusion of the vapor and Marangoni instabilities," J. Fluid Mech. **543**, 183 (2005).
[6] Y. O. Kabova, A. Alexeev, T. Gambaryan-Roisman, and P. Stephan, "Marangoni-induced deformation and rupture of a liquid film on a heated microstructured wall," Phys. Fluids **18**, 012104 (2006).
[7] S. Saprykin, P. M. J. Trevelyan, R. J. Koopmans, and S. Kalliadasis, "Free-surface thin-films over uniformly heated topography," Phys. Rev. E **75**, 026306 (2007).
[8] S. W. Joo, S. H. Davis, and S. G. Bankoff, "Long wave instabilities of heated films: Two dimensional theory of uniform layers," J. Fluid Mech. **230**, 117 (1991).
[9] S. W. Joo, S. H. Davis, and S. G. Bankoff, "A mechanism for rivulet formation in heated films," J. Fluid Mech. **321**, 279 (1996).
[10] S. Kalliadasis, E. A. Demekhin, C. Ruyer-Quil, and M. G. Velarde, "Thermocapillary instability and wave formation on a film falling down a uniformly heated plane," J. Fluid Mech. **492**, 303 (2003).
[11] P. M. J. Trevelyan and S. Kalliadasis, "Wave dynamics on a thin-liquid film falling down a heated wall," J. Eng. Math. **50**, 177 (2004).
[12] B. J. Benney, "Long waves in liquid films," J. Math. Phys. (Cambridge, Mass.) **45**, 150 (1966).
[13] C. Ruyer-Quil, B. Scheid, S. Kalliadasis, M. G. Velarde, and R. K. Zeytounian, "Thermocapillary long waves in a liquid film flow. Part 1. Low-dimensional formulation," J. Fluid Mech. **538**, 199 (2005).
[14] B. Scheid, C. Ruyer-Quil, S. Kalliadasis, M. G. Velarde, and R. K. Zeytounian, "Thermocapillary long waves in a liquid film flow. Part 2. Linear stability and nonlinear waves," J. Fluid Mech. **538**, 223 (2005).
[15] B. Scheid, C. Ruyer-Quil, U. Thiele, O. A. Kabov, J. C. Legros, and P. Colinet, "Validity domain of the Benney equation including the Marangoni effect for closed and open flows," J. Fluid Mech. **527**, 303 (2005).
[16] B. Scheid, A. Oron, P. Colinet, U. Thiele, and J. C. Legros, "Nonlinear evolution of nonuniformly heated falling liquid films," Phys. Fluids **14**, 4130 (2002).
[17] B. Scheid, O. A. Kabov, C. Minetti, P. Colinet, and J. C. Legros, "Measurement of free surface deformation by reflectance-Schlieren method," in *Proceedings of the Third European Thermal-Science Conference*, Heidelberg, Germany, edited by E. W. P. Hahne, W. Heidemann, and K. Spindler (Edizioni ETS, Pisa, 2000), Vol. 2, pp. 651–657.
[18] E. A. Demekhin, S. Kalliadasis, and M. G. Velarde, "Suppressing falling film instabilities by Marangoni forces," Phys. Fluids **18**, 042111 (2006).
[19] S. Miladinova, S. Slavtchev, G. Lebon, and J. C. Legros, "Long-wave instabilities of non-uniformly heated falling films," J. Fluid Mech. **453**, 153 (2002).
[20] S. Miladinova, D. Staykova, G. Lebon, and B. Scheid, "Effect of nonuniform wall heating on the three-dimensional instability of falling films," Acta Mech. **156**, 79 (2002).
[21] A. Mukhopadhyay and A. Mukhopadhyay, "Nonlinear stability of viscous film flowing down an inclined plane with linear temperature variation," J. Phys. D **40**, 5683 (2007).
[22] S. Miladinova and G. Lebon, "Effects of nonuniform heating and thermocapillarity in evaporating films falling down an inclined plate," Acta Mech. **174**, 33 (2005).
[23] J. M. Skotheim, U. Thiele, and B. Scheid, "On the instability of a falling film to localized heating," J. Fluid Mech. **475**, 1 (2003).
[24] S. Kalliadasis, A. Kiyashko, and E. A. Demekhin, "Marangoni instability of a thin liquid film heated from below by a local heat source," J. Fluid Mech. **475**, 377 (2003).
[25] A. M. Frank and O. A. Kabov, "Thermocapillary structure formation in a falling film: Experiment and calculations," Phys. Fluids **18**, 032107 (2006).
[26] N. Tiwari and J. M. Davis, "Linear stability and transient dynamics of non-inertial coating flows over locally heated surfaces," Phys. Rev. E **76**, 056306 (2007).
[27] O. A. Kabov, I. V. Marchuk, and V. M. Chupin, "Thermochemical imaging study of the liquid film flowing on a vertical surface with local heat source," Russ. J. Eng. Thermophys. **6**, 105 (1996).
[28] O. A. Kabov, "Formation of regular structures in a falling liquid film upon local heating," Thermophys. Aeromechanics **5**, 547 (1998).
[29] O. A. Kabov, I. V. Marchuk, A. V. Muzykantov, J. C. Legros, E. Istasse, and J. L. Dewandel, "Regular structures in locally heated falling liquid films," in *Proceedings of the Second International Symposium on Two-phase Flow Modelling and Experimentation*, edited by G. P. Celata, P. DiMarco, and R. K. Shah (Edizioni ETS, Pisa, 1999), Vol. 2, pp. 1225–1233.
[30] S. Kalliadasis and G. M. Homsy, "Stability of free-surface thin-film flows over topography," J. Fluid Mech. **448**, 387 (2001).
[31] J. M. Davis and S. M. Troian, "Generalized linear stability of noninertial coating flows over topographical features," Phys. Fluids **17**, 072103 (2005).
[32] R. D. Deegan, O. Bakajin, T. F. Dupont, G. Huber, S. R. Nagel, and T. A. Witten, "Capillary flow as the cause of ring stains from dried liquid drops," Nature (London) **389**, 827 (1997).
[33] R. D. Deegan, O. Bakajin, T. F. Dupont, G. Huber, S. R. Nagel, and T. A. Witten, "Contact line deposit in an evaporating drop," Phys. Rev. E **62**, 756 (2000).
[34] M. Cachile, O. Benichou, C. Poulard, and A. M. Cazabat, "Evaporating droplets," Langmuir **18**, 8070 (2002).
[35] C. Poulard, O. Benichou, and A. M. Cazabat, "Freely receding evaporating droplets," Langmuir **19**, 8828 (2003).
[36] C. A. Ward and D. Stanga, "Interfacial conditions during evaporation or condensation of water," Phys. Rev. E **64**, 051509 (2001).
[37] R. Marek and J. Straub, "Analysis of the evaporation coefficient and the condensation coefficient of water," Int. J. Heat Mass Transfer **44**, 39 (2001).
[38] D. M. Anderson and S. H. Davis, "The spreading of volatile liquid droplets on heated surfaces," Phys. Fluids **7**, 248 (1995).
[39] J. R. Maa, "Evaporation coefficients of liquids," Ind. Eng. Chem. Fundam. **6**, 504 (1967).

[40]H. J. Palmer, "The hydrodynamic stability of rapidly evaporating liquids at reduced pressure," J. Fluid Mech. **75**, 487 (1976).
[41]J. M. Smith, H. C. V. Ness, and M. M. Abbott, *Introduction to Chemical Engineering Thermodynamics*, 5th ed. (McGraw-Hill, New York, 1996).
[42]E. L. Cussler, *Diffusion: Mass Transfer in Fluid Systems*, 2nd ed. (Cambridge University Press, New York, 1997).
[43]S. Kalliadasis, C. Bielarz, and G. M. Homsy, "Steady free-surface thin film flows over topography," Phys. Fluids **12**, 1889 (2000).
[44]M. A. Spaid and G. M. Homsy, "Stability of Newtonian and viscoelastic dynamic contact lines," Phys. Fluids **8**, 460 (1996).
[45]O. A. Kabov and E. Chinnov, "Heat transfer from a local heat source to a subcooled falling liquid film evaporating in a vapor-gas medium," Russ. J. Eng. Thermophys. **7**, 1 (1997).
[46]C. Bielarz and S. Kalliadasis, "Time-dependent free-surface thin film flows over topography," Phys. Fluids **15**, 2512 (2003).
[47]O. A. Kabov, B. Scheid, A. Sharina, and J. C. Legros, "Thermocapillary convection in a falling thin liquid film locally heated," in *Proceedings of the Fifth World Conference on Experimental Heat Transfer, Fluid Mechanics and Thermodynamics*, Thessaloniki, Greece, edited by G. P. Celata, P. Di Marco, A. Goulas, and A. Mariani (Edizioni ETS, Pisa, 2001), Vol. 3, pp. 2007–2012.